MASTER THESIS

Microfluidic Biosensing using Giant Magnetoresistance Sensors

Issue date: 01/10/2014

Submitted at the Faculty of Electrical Engineering, Vienna University of Technology in partial fulfillment of the requirements for the degree of Biomedical Engineering, Master of Sciences (Diplomingeneur)

Under the supervision of

Ao.Univ.Prof. Dr. Franz Keplinger
Dr. Ioanna Giouroudi
Dipl.-Ing. Georgios Kokkinis

By

Murad Jamalieh, BSc.
Mat.Nr. 1129178
Gumpendorferstraße 39/553, 1060 Wien

October, 2014

Abstract

In this thesis, an integrated microfluidic biosensing system using GMR sensors for detecting pathogens according to their velocity in a static fluid is presented. Current carrying conductors are used to displace magnetic microparticles, which are used to label the pathogens, along the detection chamber.

Specifically, the magnetic particle (MP) volume increases once a pathogen is attached to its functionalized surface (LMP).

If the bare MPs and the LMPs, with the increased non-magnetic volume, are displaced over a certain distance by the same external magnetic field the LMP will travel this distance slower than the bare MP.

The velocity of the LMP inside the detection channel is measured and compared to the velocity of the MP inside the reference channel.

A GMR sensor is positioned at the inlet of the reference and detection channels respectively and it registers a change in the resistance once the MP and the LMP are introduced.

Then they are being accelerated by the magnetic field generated by the current carrying conductors. Once they reach the outlets the GMR sensor positioned there registers a change in the resistance. By knowing the time between the inlet and outlet recorded signals and the traveled distance the velocities of the MP and LMP are calculated.

This thesis concentrated on creating an improved measurement system replacing a more expensive bulky device with a cheaper, faster and easier technique. The developed technique uses a PC sound card and MATLAB script to process the signal. Also electronics that will help reducing the effect of thermal fluctuations on the signal by controlling the sensor current flow were developed.

Experiments on detecting only a single MP were carried out successfully and a proof of concept of detecting multiple bare MPs and magnetically label E. coli (LMPs) is presented.

Table of Contents

Acknowledgments

I would like to use this opportunity to deeply express gratefulness to my parents Aziz Jamalieh and Mary Bahdousheh for their great contribution, good influence and support throughout my life.

I wish to give my appreciation to Ao.Univ.Prof. Dr. Franz Keplinger for giving me the opportunity to work in such a great field in this institute. I particularly thank and appreciate Dr.Ioanna Giouroudi for her great organization and was pleased to work under her supervision. I also thank Dipl.-Ing. Georgios Kokkinis for his support and effort to guide me through experiments and overall lab work.

Additionally, I'm pleased to work in this institute as it has a very friendly and pleasant environment with its appreciable ladies and gentlemen.

At the end, I wish all who contributed, worked and will work on the accomplishment of this project a godly blessing.

1. Introduction

Magnetism has been playing a great role in the development of sensors, as it provides neat methods for probing and measuring quantities (e.g. temperature, resistance, distance … etc.) by noncontact means. Due to the remarkable advances in microsystems technology magnetic sensors can be miniaturized and thus integrated on a single chip together with their electronics. These miniaturization possibilities make them a perfect fit for biosensing applications.

In parallel, magnetic micro- and nanoparticles are being widely used in life sciences and biomedicine e.g. cell temperature, DNA sequencing … etc.

Due to their small size they can be easily used to label cells, pathogens and other biomolecules. Their stray field can then be detected by miniaturized magnetic sensors.

The most recent biosensing methods focus on Lab-on-a-Chip (LOC) systems; these devices are getting smaller and easier to use by time. The goal of such devices is to act as a portable commercial or end user suited devices to be used by non-scientific staff. For example, portable devices that measure blood sugar concentration are widely used by diabetes patients and healthy people who can find it in their local pharmacies.

This thesis is a part of a 3 years project that started in September 2012 and has the goal to fabricate an efficient biosensing diagnostic device, which can be used for quality control as well as medical diagnostics. The project is under the name "Microfluidics for the Rapid Detection of Pathogens Using Giant Magnetoresistance Sensors" and is supported by the Austrian Science Fund (FWF – Fonds zur Förderung der wissenschaftlichen Forschung), Project Nr. P24372-N19.

This thesis will introduce a new measurement method for the proposed system which could be less complicated and portable. A theoretical explanation of all parts and the materials used in our biosensing device will be explained along with simple equations that describe the governing mathematics behind some of the incorporated techniques. Additionally, the developed electronics that will be used to control the device's current flow to help stabilizing the measurement will be presented and proof of concept experiments will be discussed.

2. Theory

In Section 2.1 Superparamagnetism, the effect on which the properties of the magnetic particles used in the presented biosensing system rely, will be shortly explained. In Section 2.2 the working principle of the Magnetoresistive sensors, used to detect the magnetic particles in the presented system, will be described. Relevant microfluidic terms are defined in Section 2.3. In Section 2.4. existing state of the art magnetic biosensors are presented and the advantages of the proposed method are explained.

2.1 Superparamagnetism

Superparamagnetism is an effect which appears in ferromagnetic or ferrimagnetic nanoparticles [1] Below the Curie or Néel temperature particles that have linear dimensions less than 20nm will consist of a single magnetic domain. That means that such particles will be in a state of uniform magnetization at any field [2-4]. In order to divide themselves into magnetic domains they would need higher energy than the energy needed to remain in a single magnetic domain formation because of their small size.
Due to the magnetic anisotropy, the magnetic moment of the nanoparticle usually has two stable orientations (which define the easy axis of the nanoparticle) and is separated by an energy barrier. This barrier is proportional to the volume of the particle. At any finite temperature T, the total magnetic moment of the nanoparticle will fluctuate with a finite probability that the moment will flip from one easy direction to another. The mean time between two flips is called the thermal relaxation time τ and is given by Equation (2.1):

$$\tau = \tau_0 e \frac{K_u V}{kT} \tag{2.1}$$

Where kT is the thermal energy barrier at temperature T (k is the Boltzmann constant) and $K_u V$ is the energy barrier for magnetization reversal of a magnetic particle of uniaxial anisotropy K_u and volume V.

Such particles behave similar to paramagnetic following the Langévin model Equation (2.2):

$$M = Nm(\coth a - \frac{1}{a}) \tag{2.2}$$

Where m is the magnetic moment of the particle, N the number of magnetic moments per unit volume and $a = \frac{\mu_0 mH}{K_B T}$ is the ratio of the two energy terms.

The difference compared to paramagnetic materials is that superparamagnetic particles can align and reach saturation at relatively low fields and their magnetization can be much greater than that of ordinary paramagnetic materials [3].
For small particles at room temperature the energy barrier becomes comparable to the thermal energy kT; as the size of the particle decreases the magnetic anisotropy energy per particle, which is responsible for holding the magnetic moment along certain directions, becomes comparable to the thermal energy. Under these conditions, the thermal fluctuations induce random flipping of the magnetic moment with time. Consequently, the particles behave as superparamagnetic; the magnetization curve exhibits no hysteresis and thus no remanent magnetization M_r is present. Additionally, energy absorption due to Néel relaxation occurs in such nanoparticles. When an external alternating magnetic field is applied, the magnetic dipole moments of the nanoparticles will be rapidly reoriented. This depends on the frequency and strength of the applied field, the temperature and the size of the nanoparticles.

2.1.1 Magnetic Particles

Magnetic nanoparticles exhibit unique optical, electric and magnetic properties which can be very useful in life sciences and biomedicine; these properties strongly depend on their dimensions, mostly below 100 nm, and their surface area characteristics. Such types of nanoparticles have several advantages; for example, their controllable size which ranges from a few nanometers up to hundreds of nanometers is comparable to that of biological entities (e.g., viruses, bacteria, cells, genes *etc.*) and therefore enabling their coupling [5]. Once the surface of the nanoparticles is coated with bioactive ligands they can bind and interact with biological entities thus providing a key method of labeling or addressing these entities. Another major advantage is their magnetic nature; they can be controlled and manipulated by an external magnetic field gradient [6, 7]. The recent developments in nanotechnology and biotechnology enabled this modulation and tailoring of their composition, size, surface functionalization and magnetic properties. Moreover, it is possible to fabricate particles with sizes in the micrometer range simply by encapsulating the magnetic nanoparticles in a polymer matrix during fabrication, thus sustaining their superparamagnetic properties. Superparamagnetic nanoparticles are usually composed of ferrite particles (Iron Oxide Fe_3O_4) encapsulated in a polymer matrix.

The usage of polymer matrix also acts as a functionalization layer for further conjugation with bioactive molecules or targeting ligands by means of different types of bonds (antibodies, adsorption and covalent bond) using e.g., carboxylic or amino groups.

In addition, MPs can be functionalized with inorganic metallic materials such as gold [8] or oxide materials (e.g., silica) [9].These functionalization techniques enable the particles to be bonded to cells, biomolecules, radionuclides and many other molecules depending on the field of work.

In this thesis, the used particles were hydrophilic (with a diameter of 2.8 µm) coated with carboxylic acid (Figure 2.1) allowing covalent amide bonds to be formed with proteins/peptides; the containing matrix is PEG (Polyethylene glycol) which has the advantage of low toxicity Figure 2.2.

Figure 2.1: Photo of a small bottle of Dynabeads® M-270 carboxylic acid magnetic particles contained in a liquid solution.

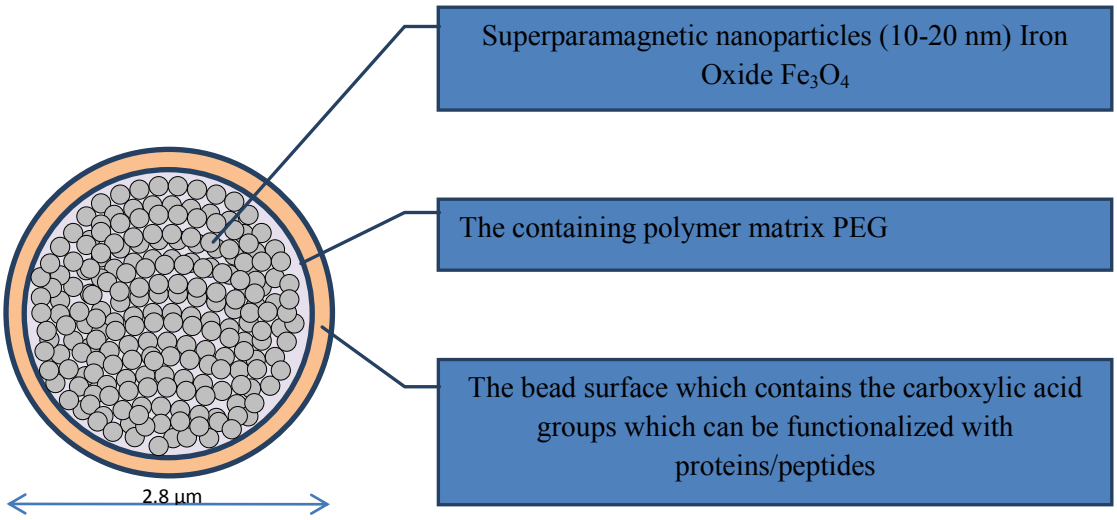

Figure 2.2: Cross section schematic of a superparamagnetic particle.

Around the superparamagnetic particles a so-called stray field is generated only upon application of an externally applied magnetic field H.
The detection of magnetic particles in static fluids or under fluidic flow requires sensors with high sensitivity to magnetic fields in the range of 1 mT and below [2, 10, 11, 13]. Chapter 2.2 presents the working principle of such highly sensitive magnetic sensors, which are used in biosensing systems for the detection of magnetic micro- and nanoparticles.

2.2 The Magnetoresistance effect (MR)

Magnetoresistance (MR) is the effect during which a change of the material's electrical resistance will occur when an external magnetic field is applied to it. This effect was first discovered in 1851 by *William Thomson* a British mathematical physicist and an engineer who is known by *Lord Kelvin* for determining the correct value of the absolute zero as approximately −273.15 Celsius.

Even though the MR effect worked *Kelvin* could not get a change in resistance of more than 5% and this effect is called the ordinary magneto resistance (OMR).

However, the progress of modern microelectronics and solid-state technology in the late 20th century enabled the broad applications of the MR effect in industrial sensors with high sensitivity and wide dynamic range as well as in data storage devices [2, 14].
The basic principle of the MR effect is described by Equation (2.3):

$$R = f(B) \tag{2.3}$$

It is the variation of a material's resistance R as a function of the externally applied magnetic field B. The application of a magnetic field to a region which contains moving electrons will cause a change in their trajectories due to the Lorentz force. This yields a change of the effective resistance of the medium containing the electrons [14]. It should be mentioned that the change in resistance is expected to be

different for a current flowing parallel to the field from that of a current flowing across the field. The usual figure of merit for magnetoresistance is the MR ratio commonly defined by Equation (2.4):

$$MR\% = \frac{R_{(H = H_{sat})} - R_{(H = 0)}}{R_{(H = 0)}} \tag{2.4}$$

Where H_{sat} is the saturation field.

This indicates the maximum signal that can be obtained from the sensor. The ability of the MR sensors to detect very weak magnetic fields (nT) at room temperature makes them very attractive for biomedical applications and there is an extended scientific interest in designing and developing magnetoresistive biochips e.g., for detecting single molecular interactions [15–22]. These applications are based on the giant magnetoresistance (GMR) effect (GMR multilayers and spin valves) and the tunneling magnetoresistance (TMR) effect [23, 24].

2.2.1 The Giant Magnetoresistance effect (GMR)

Related to the MR effect GMR effect enhances the MR effect by showing great resistance change for the defined resistor. (ΔR/R) ratios can go up to 65% in room temperature in comparison to a 6% (ΔR/R) in ordinary magnetoresistors [25].

A typical GMR structure consists of a pair of ferromagnetic thin film layers, usually taken from the transition metals (Fe, Co, Ni), separated by a non-magnetic conducting layer e.g. Cr, Cu, Ag or Au. The change in the resistance of this multilayer arises when the externally applied magnetic field aligns the magnetic moments of the successive magnetic layers as shown schematically in Figure 2.3.

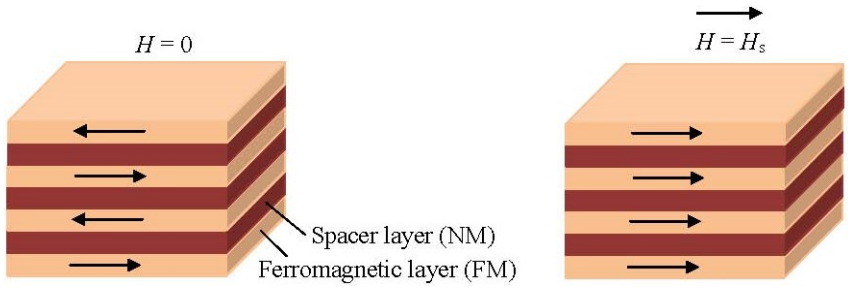

Figure 2.3: A typical giant magnetoresistance (GMR) structure.

The magnetic moments of the magnetic layers are antiparallel if an external magnetic field is not present. Once a magnetic field is applied, the magnetic moments of the magnetic layers align with respect to each other; their magnetizations are parallel. This yields a drop in the electrical resistance of the multilayer.

The GMR is deduced from the interaction of current carrying electrons and the magnetization of the host magnetic material. Once a magnetic field is present, the spin-dependent electron scattering within the structure reduces and the electrical resistance decreases [2, 18]. Figure 2.4 shows a resistor network used to model the simplest GMR structure (a trilayer structure).

The spin-up and spin-down electrons are represented by two parallel circuits and the resistance of the different layers represented by resistors is given by Equations (2.5) and (2.6):

$$R_P = \frac{R\uparrow\uparrow R\uparrow\downarrow}{R\uparrow\uparrow + R\uparrow\downarrow} \tag{2.5}$$

$$R_{AP} = \frac{R\uparrow\uparrow + R\uparrow\downarrow}{2} \tag{2.6}$$

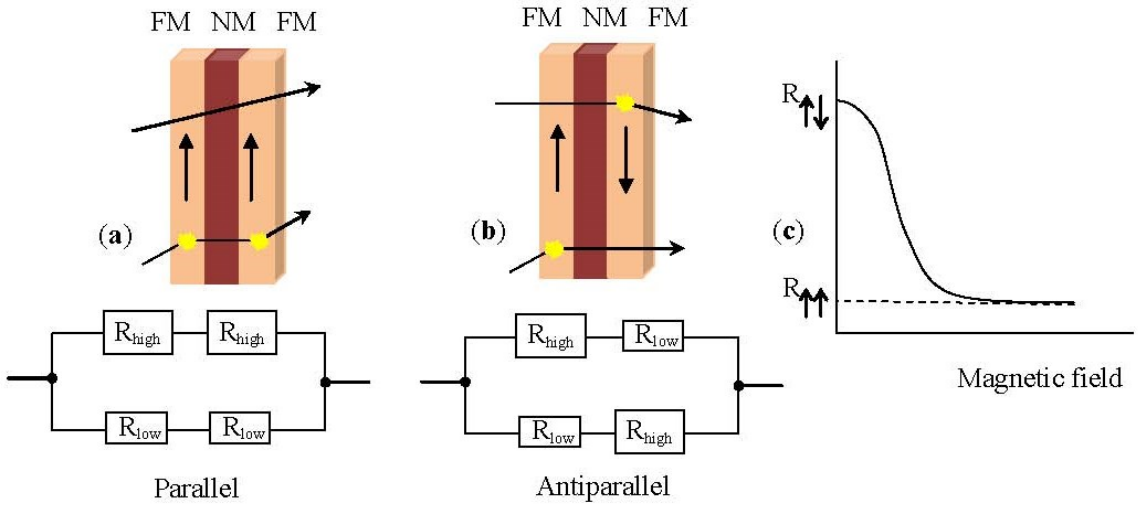

Figure 2.4: (**a**) Parallel arrangement of a trilayer structure, consisting of a pair of ferromagnetic layers (FM) separated by a non-magnetic layer (NM) with the equivalent resistor network; (**b**) Antiparallel arrangement of the same trilayer structure with the equivalent resistor network; (**c**) Graphic illustration of the resistance variation as a function of the applied magnetic field.

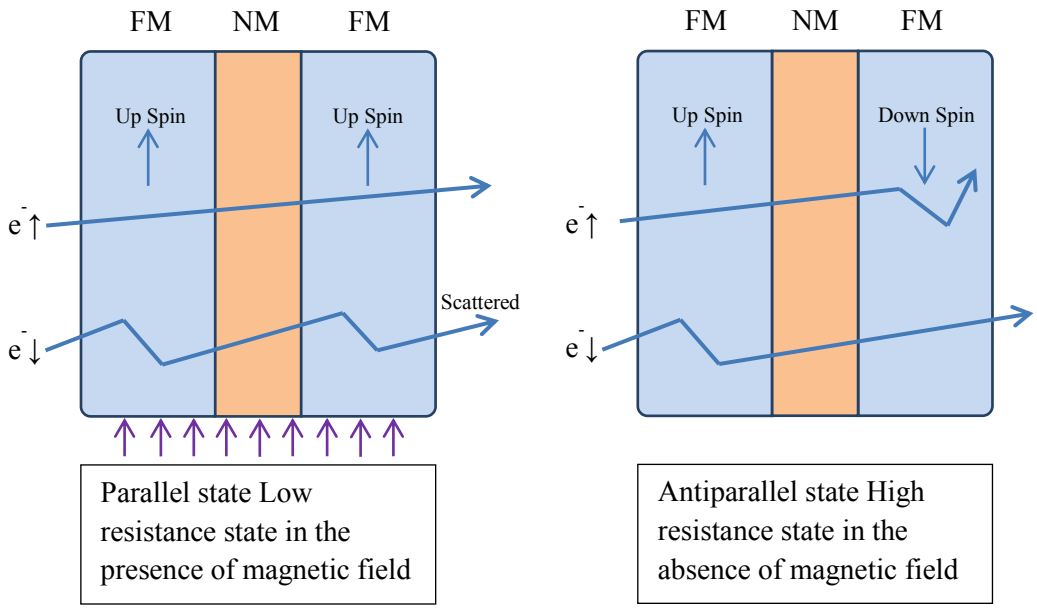

Figure 2.5: schematic of how the application of magnetic field lowers the resistance in the trilayers GMR configuration.

If we consider a magnetic multilayer structure in order for the GMR effect to occur, we should orient the magnetic moments of the magnetic layers parallel to each other (this is achieved by application of a magnetic field) and antiparallel to each other (this is achieved by removing the field).

This antiparallel alignment of the magnetization (Figure 2.4b) is accomplished by the interlayer exchange coupling [4, 5]. This coupling is mediated by the mobile electrons in the non-magnetic (NM) layer similarly to Ruderman-Kittel-Kausya-Yosida (RKKY) interaction between localized magnetic moments present in a matrix of non-magnetic metal. This interlayer exchange coupling oscillates between ferro- and antiferromagnetic as a function of the thickness of the NM layer.

Careful tuning of the thickness of the NM layer during fabrication leads to the desired antiparallel magnetization alignment at zero fields.

A main parameter to produce an effective GMR resistor is to vary the thickness of the separating layer (the non-magnetic Cr layer), that was observed in the first results obtained by *Baibich et al.* in 1988 [26].

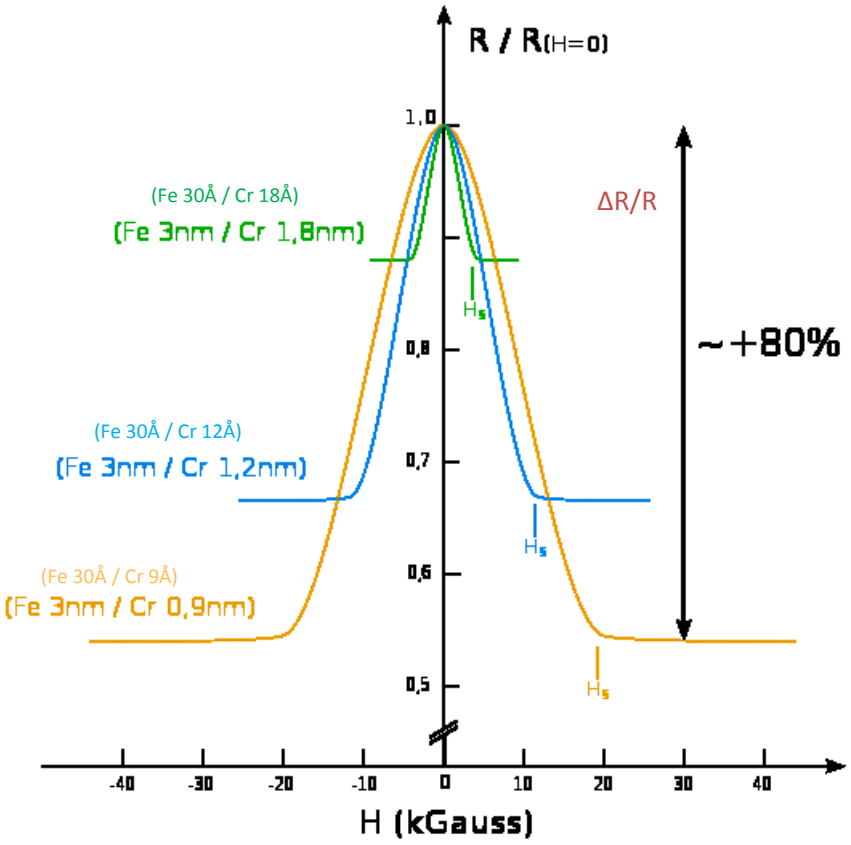

Figure 2.6: Three different plots are shown; in each plot the Cr layer thickness was decreased. The orange curve shows the greatest ΔR that was observed with the thinnest Cr layer, H_s is the saturation field after which the material will stop responding to H field change [25]

The sensor resistance can be expressed in the following equation (2.7):

$$R = R_0 + \frac{1}{2}\Delta R_{max} \sin\theta_f \tag{2.7}$$

Where:

$R_0 = R_{parallel} + \frac{1}{2}\Delta R_{max}$; Which is the sensor resistance in the orthogonal direction (when the H field is zero) Refer to R vs. H graph below.

$\Delta R_{max} = R_{antiparallel} - R_{parallel}$; Gives the maximum resistance change between ↑↓ and ↑↑ states.

θ_f; is the orientation angle of the free layer magnetization M_f with respect to the longitudinal axis of the sensor (along the sensor); (see Figure 2.7).

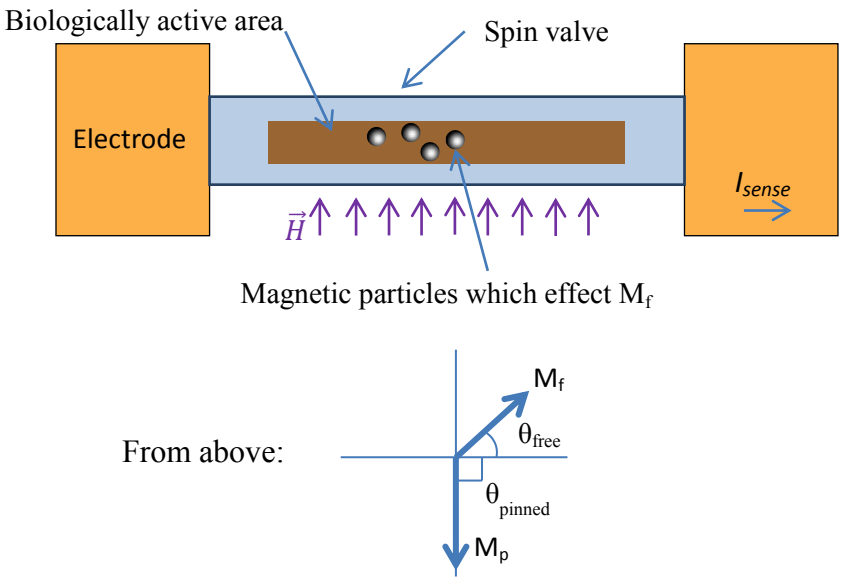

Figure 2.7: Schematic of simple GMR sensor with a constant magnetic field applied and magnetic particles being introduced or actuated through a microchannel placed on the surface of the sensor; the particles affect the overall magnetic field which varies M_f and R_{sensor} as a result. [2]

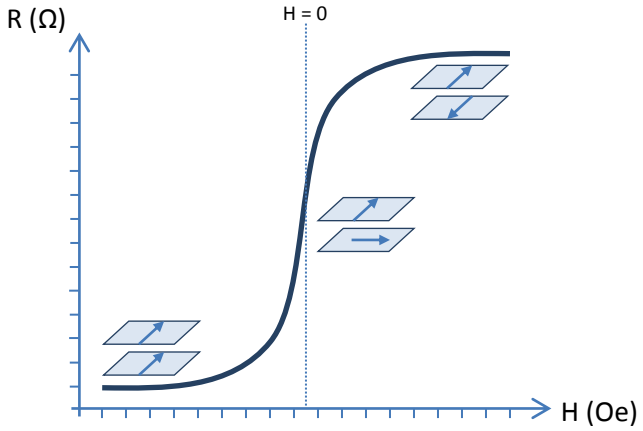

Figure 2.8: Diagram of the Resistance R (Ω) vs. H (Oe) [2]

Some of the most significant properties of the GMR sensors which make them suitable for microsystems are:

- The sensor can detect the stray field produced by a single magnetic particle, of approx. 2.8μm diameter, and it can work on a large scale of technology fields (e.g. inexpensive and highly portable devices for molecular scale analysis).

- Can be manufactured in very small dimensions thus giving the ability to be integrated in a single chip (e.g. several sensors on a silicon wafer)

- Suitable for multianalyte biodetection (i.e. different types of biomolecules can be mixed in the analyte solution and can be detected in the same measurement session).

- It can detect particles in its proximity of less than or equal to 1μm.

- Is widely used in combination with micro- or nanoparticles which can be bound to different types of molecules in an analyte sample (this method is known as magnetic tagging of bioanalytes) [2].

2.3 Magnetophoresis & Microfluidics

Magnetophoresis, a nondestructive method for selectively collecting or separating magnetic particles, is the process of magnetic particle motion in a viscous medium under the influence of a magnetic field; the viscous medium may be a magnetic or immunomagnetic liquid, and the magnetic field should be in a gradient format. The operating principle of the magnetophoresis is that the direction and velocity of the particle movement in a gradient magnetic field are determined by magnetic F_m, gravitational F_g, and drag F_d forces, therefore by selectively controlling these forces, it is possible to control the mobility of the different magnetic particles. [26]

Microfluidic techniques allow precise control of fluids and particles at the nanoliter scale and facilitate simultaneous manipulation and analysis of bioanalyte (e.g. cells) [27]. Microfluidics provide a rapidly grown platform for developing new powerful tools which facilitate fluid transport and fluid analysis on a single chip system for applications in biotechnology, life sciences, public health, pharmaceuticals and agriculture. Such microfluidic chips usually contain microvalves and micropumps in order to enable controlled fluid flow, fluid mixing and/or separation. Some of the benefits of using microfluidics in such applications are: the small sample volumes required for testing which lead to greater efficiency, parallel processing of samples and therefore fast sampling times, accurate and precise control of fluid samples as well as diverse integration of different detection methods yielding greater sensitivity, low power consumption and low production costs thus permitting disposability.

2.3.1 Laminar and turbulent flow

The most important micro-domain effect appearing in microfluidic devices is the laminar flow, which occurs when the fluid is flowing in a parallel manner to the channel boundaries without being mixed together and disturbed. That usually happens at low velocities, and small channel diameters [28]. Laminar flow is a condition in which the velocity of a particle in a fluid stream is not a random function of time. Because of the small size of microchannels, flow is almost always laminar (see Figure 2.9a) [29].

On the contrary turbulent flow occurs at higher velocities, higher channel widths and larger fluid densities, due to the drag forces within the fluid [28]. Turbulent flow is chaotic and unpredictable (i.e., it is impossible to predict the position of a particle in the fluid stream as a function of time) (see Figure 2.9b) [29].

The Reynolds number (Re) of a fluid flow describes its flow regime laminar or turbulent; the equation (2.8) which characterizes this behavior is denoted by **Reynolds number (Re)**:

$$Re = \frac{\rho D_h u}{\eta} \tag{2.8}$$

Where:

ρ; Density of the fluid.

D_h; Hydraulic diameter, depending on the shape of the channel, for non-circular ducts there is a different formula to calculate the hydraulic diameter as in Equation (2.9):

$$D_h = \frac{4 \times Cross\ Section\ Area}{Wetted\ Perimeter} \tag{2.9}$$

Cross section area is the area of the channel through which the fluid is flowing.

Wetted perimeter is the sum of the lengths of each surface in contact with the aqueous body.

u; The characteristic velocity of the fluid in the channel.

η; The dynamic viscosity of the fluid [30].

Figure 2.9a: Laminar flow scheme occurs when viscous forces overcome the inertial forces of the fluid, and usually are observed in microfluidics with $Re \ll 1$

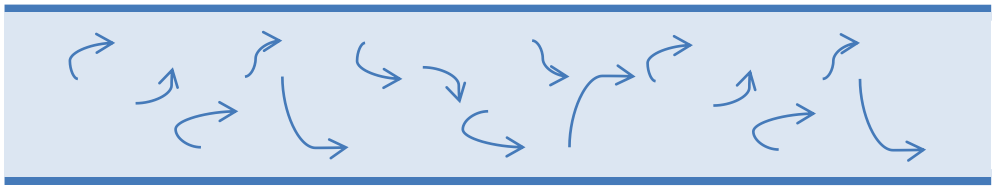

Figure 2.9b: Turbulent flow scheme occurs when inertial forces overcome the viscous forces of the fluid, and are observed with $Re \gg 1$; it is also related to the channel shape and wetted surface roughness.

Figure 2.10 shows a microfluidic chip which was fabricated at ISAS (Institut für sensor und actuator systeme) in the technical university of Vienna.

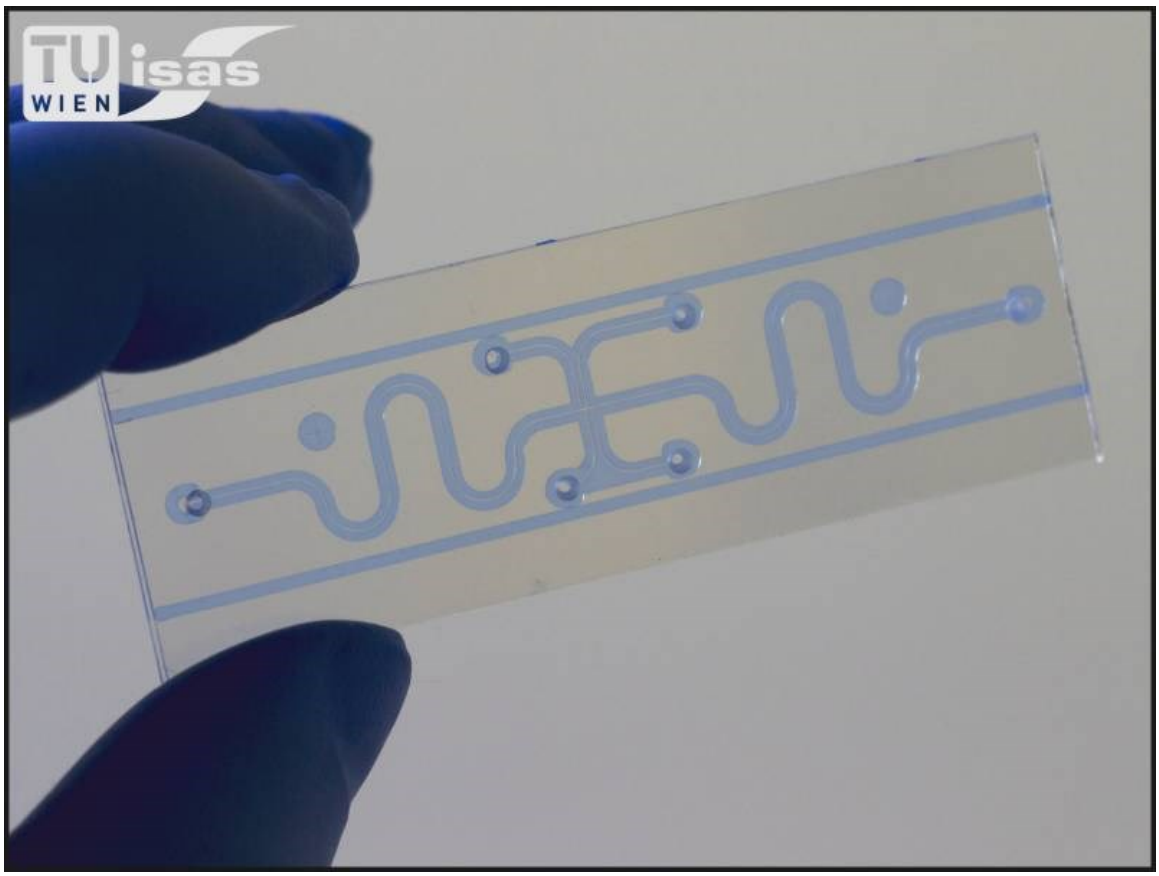

Figure 2.10: Shows a typical microfluidic chip that uses a combination of channels used to manipulate the fluid within.

3. System Design

In this chapter the design of the biosensing system for the detection of pathogens and its implementation are being described. Specifically, section 3.1 presents the working principle of the biosensor which is based on the velocity change of MPs due to a change in their non-magnetic volume by the presence of pathogens. The detection of the magnetically tagged pathogens is carried out using GMR sensors. The analytical calculations related to the working principle are reported, concerning the change in velocity when the volume of MPs changes. In section 3.2 the design of the GMR sensor is explained and a comparison between different existing MR sensors is shortly presented. Finally, section 3.3 presents the existing microfluidics fabrication technologies, including the one used for the fabricated biosensing system.

3.1 Working Principle

The biosensing system consists of a reference microfluidic channel and a detection microfluidic channel. Near the inlet and the outlet of the two channels GMR sensors are positioned. Parallel current carrying conductors are also fabricated underneath the channels in order to move the magnetically tagged pathogens from the inlet to the outlet. A data acquisition system records and saves the findings.

In our system the fluid under investigation is static. The reference channel is filled only with bare MPs whereas the detection channel is filled with MPs functionalized with ligands directed against the pathogens to be detected. If pathogens are present in the fluid then they will attach to the surface of the functionalized MPs.

This bonding of pathogens to the surface of the functionalized MPs causes an increase to their non-magnetic volume; we refer to these MPs as Loaded MPs (LMPs) as shown in Figure 3.1.

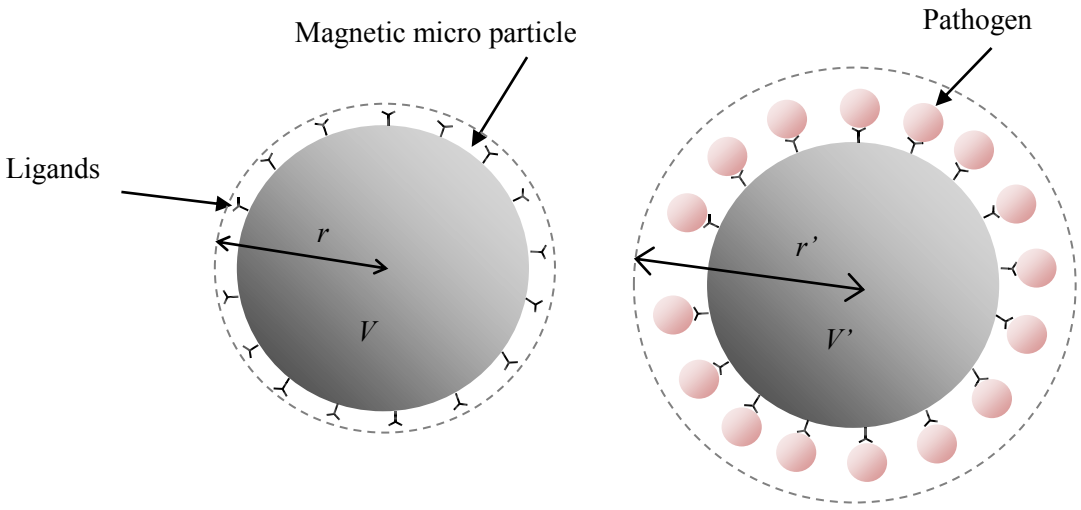

Figure 3.1: On to the left the unloaded magnetic functionalized with ligands is shown, and on the right the loaded MP with the pathogens attached to its surface; *r'* and *V'* are the total radius and volume of the LMP respectively [31-34].

The application of an external magnetic field, by means of the parallel current carrying conductors, will align the MPs with it and force them to move towards the higher magnetic field strength. The MPs in the reference channel and the LMPs in the detection channel will move with different velocities due to the drag forces associated with their overall volume in the fluid (see Figure 3.2.)

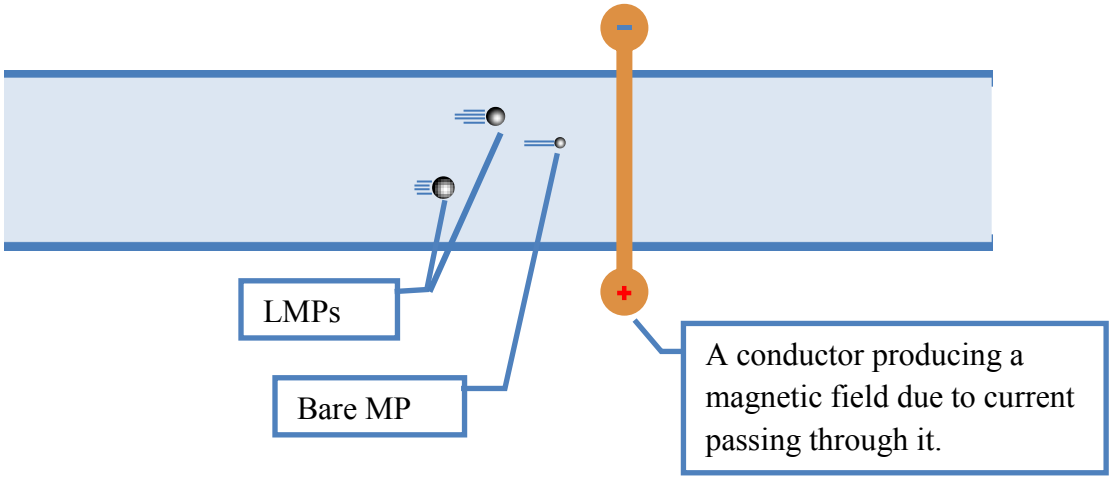

Figure 3.2: Three magnetic particles with different non-magnetic volumes moving towards the conductor at different speeds due to their different sizes are shown; the 3 different sizes can occur due to the attachment of different types of non-magnetic pathogens.

3.1.1. Analytical Calculations

In order to move an MP, a magnetic field gradient has to be applied along the x-axis; that gradient will force the MP to move towards the highest intensity magnetic field, thus a certain force is generated to pull the MP.

This approach is referred to as "Magnetophoresis". Specifically, a uniform magnetic field does not induce a translational force on the MP. It only gives rise to a torque which forces the MP to align to the direction of the applied magnetic field.

On the contrary, the magnetic force which is generated by the magnetic field gradient on a single MP is given by:

$$\vec{F}_{mag} = \frac{1}{\mu_0}\nabla(\mathrm{m}\cdot\vec{\mathrm{B}}) \tag{3.1}$$

Where:

μ_0; is the magnetic permeability in vacuum

$\vec{B}$; is the magnetic induction field vector in Tesla

m; is the magnetic moment of the MP induced by $\vec{B}$

The magnetic moment of the MP is induced by a field $\vec{B} = \mu_0 \vec{H}$ and m is expressed as

$$\vec{m} = V\chi\vec{H} \tag{3.2}$$

Where:

V; is the volume of the MP

χ; is the effective susceptibility of the MP

And because the magnetic susceptibility of the surrounding medium is assumed to be zero and there are no time varying fields or currents in the medium or MP properties we can reformulate the F_{mag} formula in the case of a superparamagnetic nanoparticle and express it by:

$$\vec{F}_{mag} = \frac{V\chi}{2\mu_0}\nabla\vec{B}^2 \tag{3.3}$$

The moving MPs experience a hydrodynamic drag force which originates from the velocity difference Δv between the MPs and the containing fluid itself; in our case the fluid is stationary. For a spherical particle with a radius r and a fluid with a low Reynolds number the drag force is expressed by:

$$F_{drag} = 6\pi\eta r\Delta v \tag{3.4}$$

Where η is the viscosity of the containing fluid.

With a static fluid and a steadily moving particle i.e. constant speed, one can calculate the flow rate of the particles. By equalizing (3.3, 3.4) we get Δv as the following:

$$\Delta v = \frac{r^2\chi}{9\mu_0\eta}\nabla\vec{B}^2 \tag{3.5}$$

In the case of loaded MPs the total radius r' will increase and this will be shown in F_{drag} equation:

$$F_{drag} = 6\pi\eta r'\Delta v \tag{3.6}$$

Where; $r' = r + 2r_p$, r_p is the radius of the attached bioanalyte [31-34].

3.2 GMR Sensor Design

The magnetic sensing system consists of multiple GMR sensing elements that will be used to detect the MP/LMP respectively as described in section 3.1; two are placed near the inlets of the reference and detection channels respectively and two are placed near the outlets of the microfluidic channels. Underneath the channels the parallel current carrying conductors are fabricated perpendicular to the x-axis of the channels, in order to move the bare MPs and the magnetically tagged pathogens (LMPs) from the inlets to the outlets.

When the MPs approach the inlet-GMR sensor a change in its resistance will occur and the measurement system will register that as a voltage change. Then the MPs will continue moving and will be accelerated to a certain velocity by the conductors towards the outlet-GMR sensor. At this point a change in the resistance of the outlet-GMR sensor will occur. The data acquisition system will then register the times when the GMRs produced their signals and from that we can calculate the velocity of each MP using the distance between the two GMRs. Figure 3.3 shows a schematic of the microfluidic biosensing system.

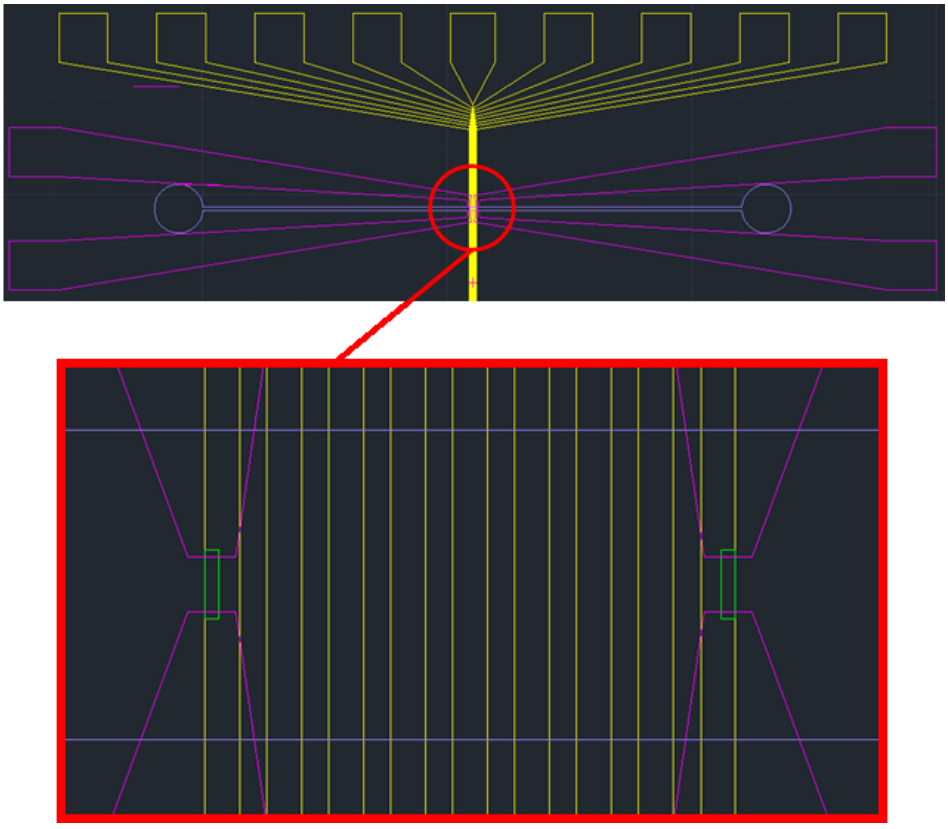

Figure 3.3: AutoCAD drawing of the biosensing system used in this thesis. The top picture shows the current carrying conductors in yellow with their contacting pads at the top, the GMR sensors connectors in pink and the microfluidic channel in purple which is not imbedded in the sensor assembly. The bottom picture is their magnification and additionally shows the two GMR sensors in green.

In Chapter 4, a detailed description of the fabricated biosensing system will be presented.

3.2.1 Existing MR sensors

An MR sensor can be found in different designs in terms of input and output parameters and the purpose of the measurement, but all types are aimed to measure the magnetic field components that affect them. One of the first useful sensors is the AMR sensor (Anisotropic Magnetoresistive) usually composed of $Ni_{80}Fe_{20}$ which exhibits a MR effect of 5% at room temperature; it's commonly used with a magnet to make the sensor reach its saturation $H_{applied} \geq H_{sensor}$ to ensure the maximal AMR effect and so it can be used as a non-contact switch replacing the ordinary miniature mechanical switches which cannot be too small and also raise a difficulty in orientation on the PCB boards (see Figure 3.4.).

Figure 3.4: An AMR sensor used to detect the closure of the mobile screen.

Another category of MR sensors are the TMR sensors (Tunnel Magnetoresistive). They are based on a quantum mechanics phenomenon; the sensor is built from two ferromagnetic layers separated by a very thin insulating layer in the nm range. If the magnetizations of the two ferromagnetic layers are aligned together with the externally applied magnetic field then electrons have a high possibility to jump from one ferromagnetic layer to the other passing through the insulating layer. This produces a two state sensor which switches between high or low resistances.

The TMR sensor development has significantly enhanced its specifications through the last 40 years by using different material combinations; the "resistance change percentage" started with 14% at 4.2Kelven in 1975 and reached about 1100% at 4.2Kelven in 2009 (600% at room temperature) [36, 37].

Table 3.1: A comparison of the specifications of each MR technology formerly mentioned, is shown [38].

Technology	Current (mA)	Size (mm)	Sensitivity (mV/V/Oe)	Dynamic Range (Oe)	Resolution (mOe)	Operating Temperature (°C)
AMR	1-10	1x1	1	0.001	0.1	<150
GMR	1-10	2x2	3	0.1 - 30	2	<150
TMR	0.001-0.01	0.5x0.5	20	0.001-200	0.1	<200

Despite the fact that TMR is the most advanced technology in the MR Field, GMR sensors are being used and tested in this thesis, taking into consideration the application, sensitivity, range of measurement, temperature, size, cost and available resources.

3.3 Microfluidic Technologies

Since 1980 different kinds of micro- and nanofluidics appeared for the purpose of transporting, mixing, separation and analysis of micro- and nanoliter analytes. Formerly such processes required large equipment and resources.

Recently different kinds of micro- and nanofluidic technologies are being investigated and will be briefly described in this section. The technology that fits this thesis purpose (Polymer Technology) was chosen considering its simplicity and functionality.

- Silicon Technology (between 1980s – 2000):

Originally developed for the Inkjet printers, works in the printing head nozzles where the Ink is conducted and dropped out on the paper. It can deliver volumes from 1 to 2 Pico liters. Even though this technology is well established and allows well defined geometries, it has a difficult bonding process to stack wafers of Si and glass and is also expensive (see Figure 3.5).

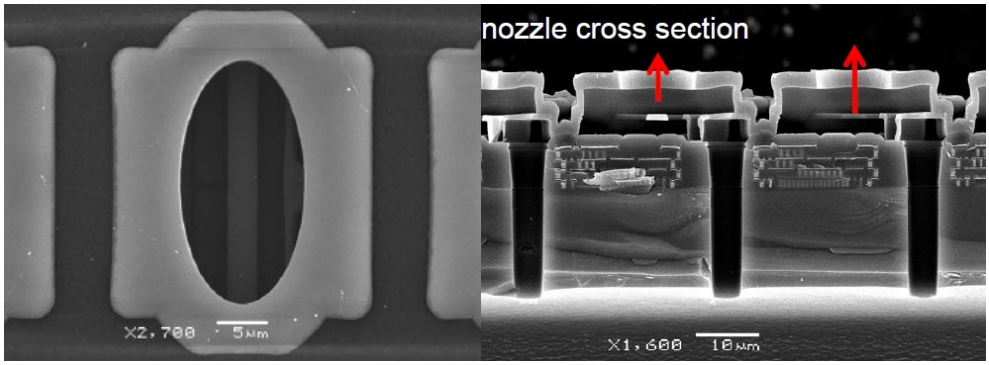

Figure 3.5: Left image shows the top side of the nozzle, right image is a cross section of more than one nozzles [35].

- LTCC (Low Temperature Co-fired Ceramic) Technology:

It is a multilayer thick layer technique that uses multiple ceramic layers stacked over each other, pattered using laser cutting and sintered (solid formed) at 900°C with thicknesses of 100 – 300 µm for each layer. This technology produces opaque structures and allows chemistry and processing of samples at higher temperatures (see Figure 3.6.).

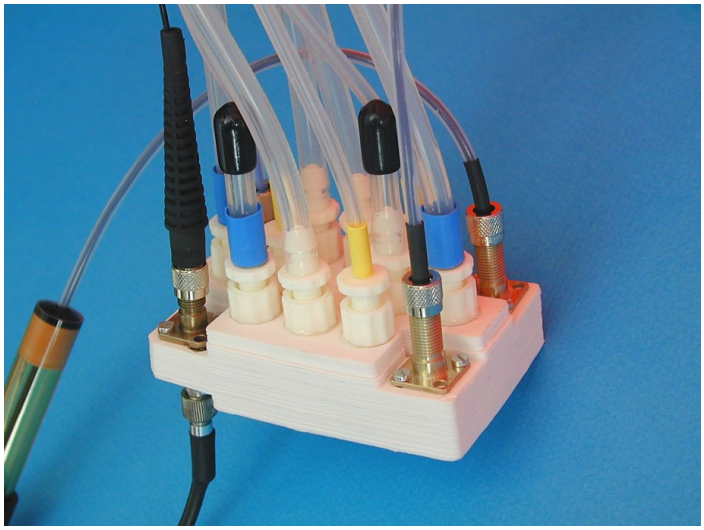

Figure 3.6: Reactor cell with integrated mixing LTCC-Stack of the reactor cell chamber, temperature control system (channels for cooling and heating media), optical fiber connections for fluorescence spectroscopy, pH- and oxygen sensors [35].

- Dry Resist:

This technology is mainly used (standard) for the Printed Circuit Board industry. It is easy to use and cheap and can produce 3D structures using repetitive layering processes as shown in Figure 3.7.

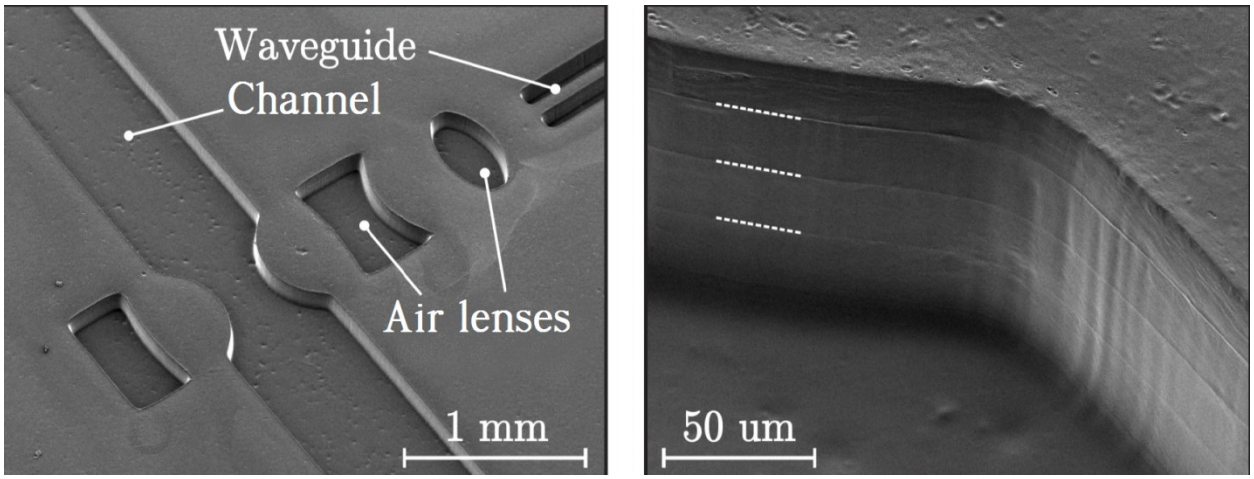

Figure 3.7: A multilayer channel system produced from multiple layers of dry resist [35].

- Paper Technology:

This method is easy to cut and extremely cheap; mainly hard paper is used and certain paths are pressed on its surface and used to guide a certain fluid (see Figure 3.8.), a useful application is in pregnancy tests.

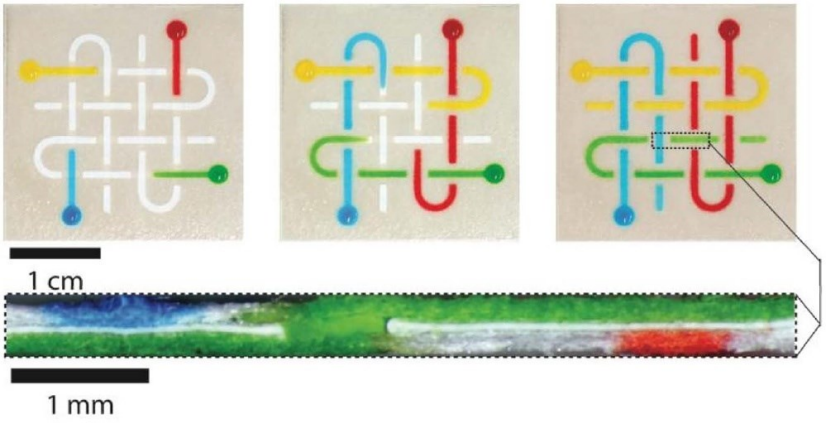

Figure 3.8: A demonstration of fluids with different colors being guided through a paper channel system [35].

- Polymer Technology (commonly used PDMS, Polydimethylsiloxan):

PDMS is a polymer that is commonly used in creating microstructures which can be microchannels for fluid transportation; it can be manufactured from a solid or a powdery state with heating stages to form a transparent rubbery-like state. PDMS is widely used because it allows well defined geometries (see Figure 3.9), it is transparent (it can be used to monitor the analyte or sample inside the channel), it can be embossed to create the desired structure and it is cheap.

In this thesis we use PDMS which proved to be a very satisfying solution. Details on the preparation, design and the production of such channels will be further discussed in chapter 4.

Figure 3.9: A microfluidic system being pealed out of its molding. Afterwards the PDMS can be placed on a sensor system to analyze the flowing samples [35].

4. Biosensing System Development and Measurements

In order to verify the working principle described in section 3.1 a microfluidic biosensing system was developed. The next sections describe the fabrication of the chip (section 4.1) as well as the experimental set-up (section 4.2) and the measurements that where conducted (section 4.3).

4.1 Fabrication

In this section the fabrication steps for the GMR sensors, the current carrying conductors and the microfluidic channels will be described in detail. The fabricated final product is a 4 inch silicon wafer with multiple biosensing chips which were cut using a diamond saw.

4.1.1 GMR Sensor

Each chip contains 4 GMR sensors and 9 current carrying conductors. Below, the GMR layers, spin-valve configuration and the fabrication process will be explained.

A spin-valve GMR configuration is fabricated in this project and it consists of a trilayer active GMR region. The following table and figure will describe the configuration and the purpose of each layer.

Table 4.1: hows the materials used in the GMR sensor and why they were chosen

Material	Thickness (Å)	Thickness (nm)	Specifications/Usage
Ta (Tantalum)	30	3	High melting point, oxidation resistance, inert, bio-inert, non-ferrous (non-magnetic) [39-42].
NiFe (Nickel-Iron Permalloy)	36	3.6	Magnetic alloy, high magnetic permeability, low coercivity, significant anisotropic Magnetoresistance [43-45].
IrMn (Iridium-Manganese)	85	8.5	Has higher pinning strength capability in higher operating temperatures in comparison to its opponent FeMn, and easily prepared [46].
CoFe (Cobalt-Iron)	23/30	2.3/3	One of the magnetic alloys and used in GMR trilayers to create the desired MR ratio.
Ru (Rubidium)	8	0.8	Used here to couple two CoFe layers to form a synthetic antiferromagnetic which makes the hard/pinned layer more resistant to high external magnetic fields which might break the pinning.
Cu (Copper)	30	3	Copper is the non-ferromagnet which makes the active GMR region and acts as a spacer between the two ferromagnetic alloys which are the spin-valve [48].

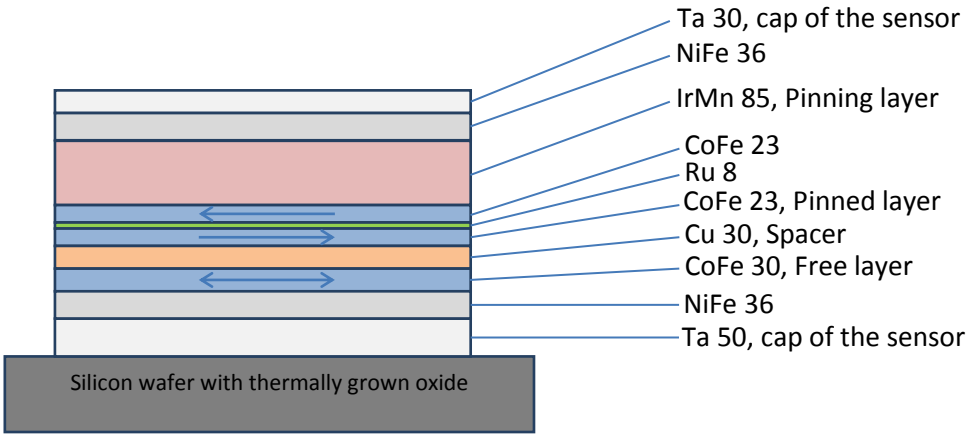

Figure 4.1: The GMR sensor and the spin-valve configuration, with the Si-wafer as the base.

The fabricated GMR sensor has the following characteristics:

- Magnetoresistance ratio of 5.23%

- Coercivity field H_c of 3.02 Oe

- The ferromagnetic coupling field of the pinning layer H_f field of 11.45 Oe

The GMR sensor was fabricated at INESC-MN Lisbon Portugal using the standard following process steps (see Figure 4.2):

a) Before any processing the GMR material is deposited on the 4" Si-wafer using sputtering ready to be defined (segmented) according to a specific design.

b) GMR structure: the wafer is coated with 1.5μm negative PR (photoresist). Then the PR is patterned using a Mask and it is exposed to UV light in the mask aligner device. Afterwards the PR is developed in a solutionto reveal the GMR microstructures.

c) In order to deposit electrodes the sides of each GMR microstructure are being removed by Ion milling.

d) The remaining PR is removed

e) Another layer of PR is spun on the wafer in order to prepare the electrode lines.

f) Al is being deposited to form the electrode lines. Lift off procedure is used to remove the extra Al using μ-strip and ultrasonic bath.

g) Silicon Nitrate passivation layer is deposited; this isolation layer is pattered and etched at the points where electrical connections are (on the edges of the whole chip).[1]

h) In order to reveal the contact pads reactive ion etching and resist stripping is used.

[1] This cross section shows only the layers where the GMR sensor is and all other electrical connections extend in between layers to the edges of the chip.

i) The current carrying conductors are being patterned on top using a mask. The conductors are patterned on the axis which goes through this page therefore its pattern will not be shown.

j) Another passivation layer (Si_3N_4 + SiO_2) is being deposited on the top of the conductors.

k) Exposure of passivation layer and connecting pads opening

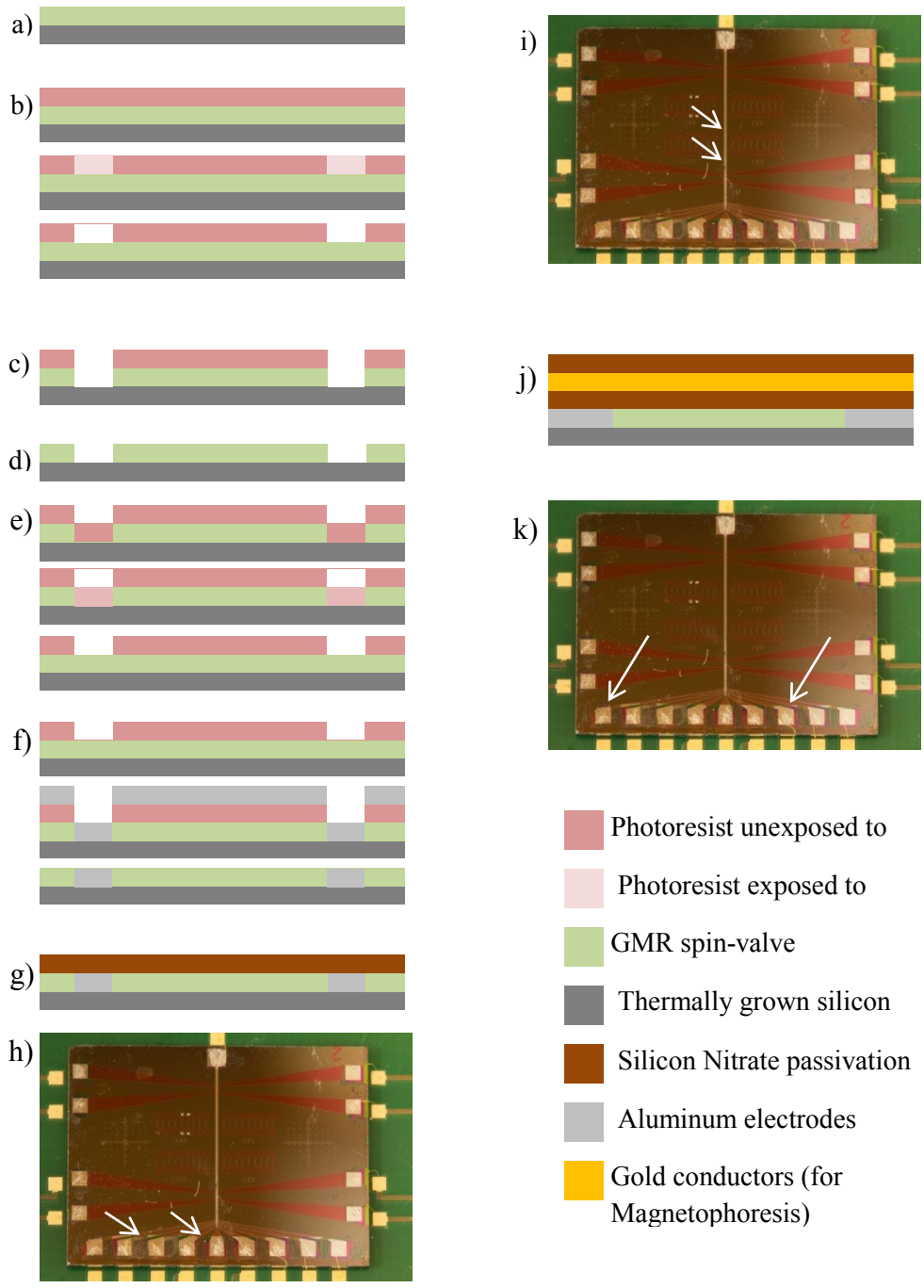

Figure 4.2: The standard fabrication steps of each layer are presented as described above.

As a last step of the fabrication procedure annealing of the whole wafer is being carried out. The wafer is annealed for 15 min at 250°C and exposed to 1 Tesla magnetic field during the annealing process (see Figure 4.3.).

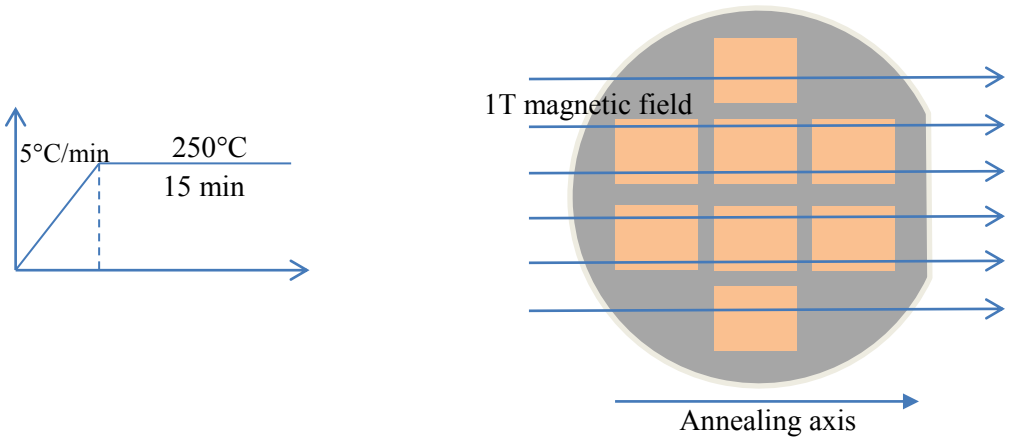

Figure 4.3: Description of the annealing process.

The annealing process starts with ramping the temperature at a rate of 5°C/min till reaching 250°C then annealing it for 15 min under 1T field in the direction of its annealing axis. After that, the wafer is cooled down to 80°C at1x10^{-6} Torr vacuum with the magnetic field applied until the end of the process.

This process is specifically called "Magnetic thermal annealing"; in which the benefits of the thermal and magnetic effects are incorporated; in the common thermal annealing, the material will experience hardening of its lattice and the atoms will diffuse more easily and find their proper locations. This will lead to relieve the internal stresses, refine the structure by making it more homogeneous and also remove the shape as well as structural deformities [48].

On the other hand the applied magnetic field of 1 Tesla is mainly used to pin the magnetization direction of one of the FM layers in the GMR spin-valve to the annealing axis so that this layer acts as a reference to the other free FM layer.

One of the most important effects of the magnetic thermal annealing is the reorientation of the easy axis in a FM material, or the axis of spontaneous magnetization. In any FM material, the easy axis is primarily determined by the lattice structure (in some cases, by the shape or the internal strain of a solid). For example, if the lattice shows specific symmetry, the easy axis will normally reflect this symmetry. However, if the lattice has many deformities, there may not be any major global symmetry, and the spontaneous magnetization will be weakened or randomized. If a deformed FM lattice is annealed at a high temperature, the spins of each individual atom will align with the externally applied field and when maintained at a high temperature, this spin-field interaction will begin to reorganize the lattice, due to the spin-orbital interaction (i.e. the interaction between the atomic orbitals and the electron spins inside a crystal lattice). Eventually the system will attain equilibrium within this field, causing a lattice reorientation such that the easy axis becomes parallel to the applied field. When the temperature is

reduced the lattice will become “locked or frozen” and the material will attain a new magnetization direction with a much robust and well-defined easy axis as shown in Figure 4.4. and Figure 4.5. [48].

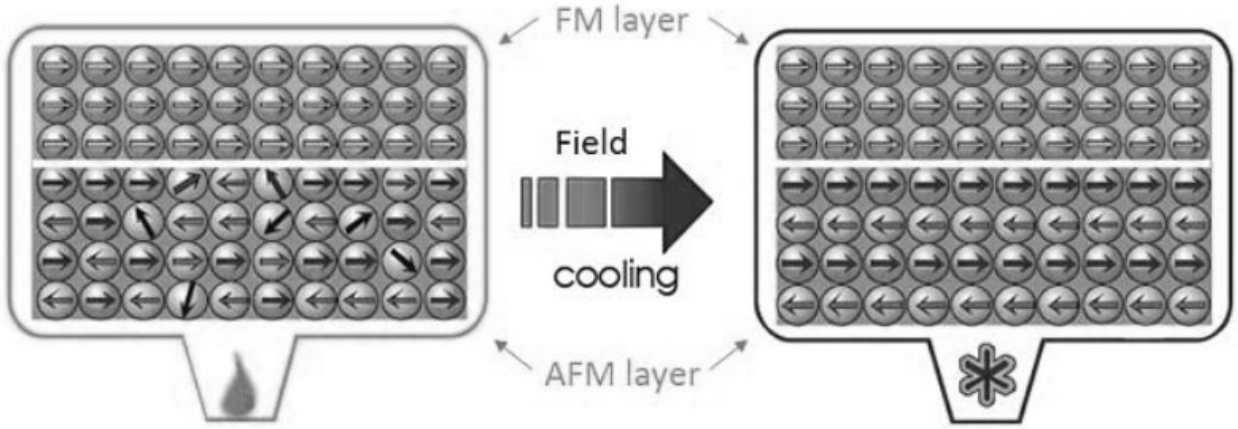

Figure 4.4: After magnetic thermal annealing, an AFM layers becomes much more ordered and pins the adjacent FM layer [48].

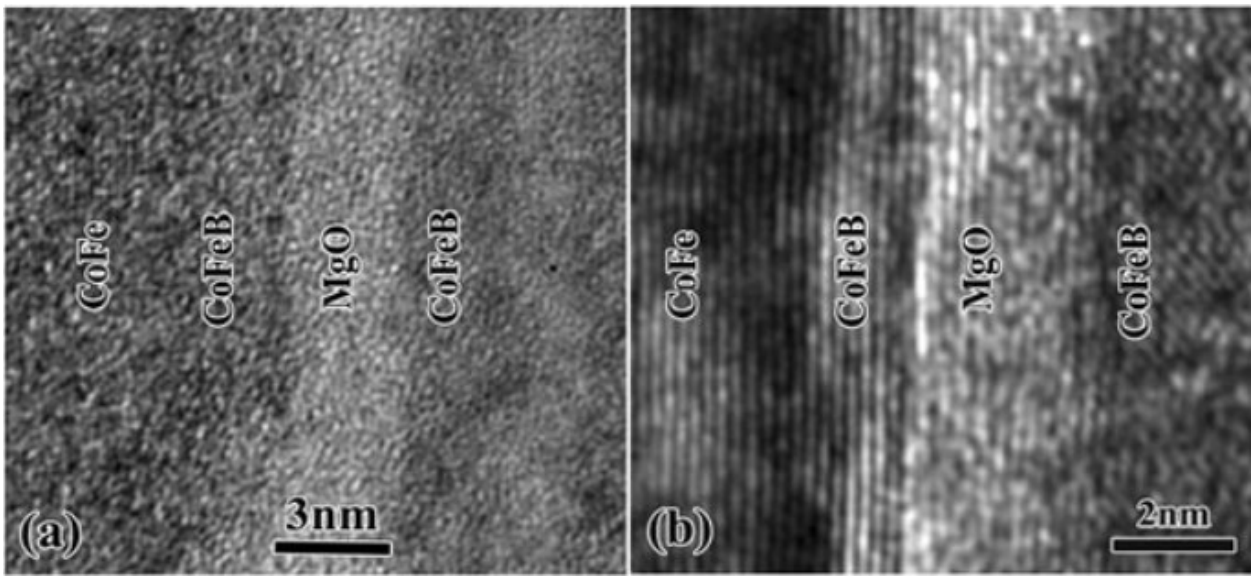

Figure 4.5: Cross sectional images of a magnetic tunneling junction layers. (a) Disordered materials before annealing. (b) Layers much less disordered after annealing [48].

4.1.2 Fabrication of the PDMS Microfluidic Channel

A typical microfluidic channel is a capillary that allows the usage of very small volumes of fluids which contain the substances that are ready for analysis. A common microfluidic channel has lateral dimensions which range from 10 to 1000 μm [49].

A widely used component of microfluidic fabrication is PDMS polymer (Polydimethylsiloxane),which has the chemical formula $CH_3[Si(CH_3)_2O]_nSi(CH_3)_3$, where n is the number of repeating monomer $[SiO(CH_3)_2]$ units [50]. PDMS is chosen for its simple and easy preparation; it is commonly used in research because it offers a good safe environment; it does not react with common chemicals and it is also transparent which allows for sample optical monitoring and image analysis (e.g. optical spectroscopic techniques).

PDMS itself is non-biodegradable. Nevertheless, it is environmentally safe as no harmful effects have been recorded on organisms in the environment; the polymer is absorbed in waste water treatment facilities and its degradation is catalyzed by various clays [50].

To fabricate a microfluidic channel different methods can be used. i) **Soft lithography**; begins with creating simple or 2D inverted shape of the channel structure using a photoresist. After that, the PDMS viscous liquid is poured over the structure and cured to create the channels. ii) **3D fabrication by stacking multiple layers**; this method produces more complex channel shapes by creating 2D structures, then aligning and stacking them over each other. iii) **Solid-object printing**; the solid mold (master) from a thermoplastic material is used to create a final shape which is the inverted shape of the micro structures required is printed [49].

In this thesis soft lithography is used for its simplicity and the availability of the equipment to achieve the process. The steps of creating the desired channel for the fabricated GMR sensor will be explained in the following pages.

Before preparing the PDMS a master (or mold) should be designed and created. First of all, a mask is designed which corresponds to the required channel dimensions, usually using CAD software (see Figure 4.6). This design is then printed or deposited on a specific glass surface. After that a silicon wafer is used as the mold base and a layer of photoresist (PR) is placed on the top of the silicon wafer; the photoresist can either be a dry thin-film (Ordyl type) which comes in different thicknesses and requires heat lamination over the Si-wafer or the liquid type which can be spinned over the Si-wafer for a specific time in order to get the required thickness (which will later determine the channel height). The laminated wafer-resist structure will then be placed in the mask aligner device with the designed mask inserted in it. Then it is exposed to UV light for a specific duration (see Figure 4.7); this UV light is projected on the PR surface according to the mask design, and UV light will harden or soften the PR depending on its type. Finally, the wafer will be inserted in a solution that etches the soft PR material revealing the inverted channel structure over the Si-wafer.

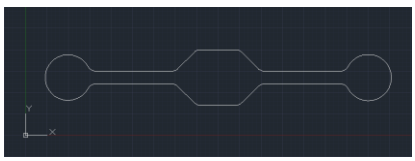

Figure 4.6: CAD drawing of the used microfluidic channel with an inlet, outlet and a chamber to allow sample observation under the microscope. The drawing can be used to create the mask which will project a UV light drawing on the PR surface.

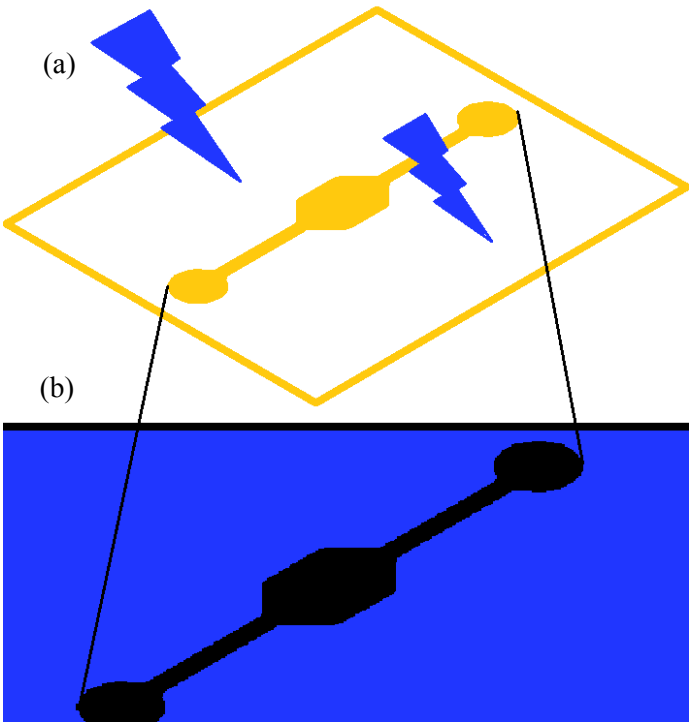

Figure 4.7: (a) High resolution photomask exposed to UV light from the mask aligner. (b) Shadow of the mask projected on the PR. The exposed areas of the PR will soften and therefore the PR can easily be dissolved (i.e. etched) using a chemical solvent. As a result the only remaining thing on the Si-wafer is the protruding structure made form PR material.

PDMS comes as two components, the base and a curing agent. The silicon hydrid groups present in the curing agent react with the vinyl groups present in the base and form a cross-linked elastomeric solid under certain curing temperature. Following are the standard preparation steps (see Figure 4.8.):

a) To create a replica using the master (mold) we mix the PDMS components together with a ratio of 10:1 (volume to volume of base to curing agent) to produce a pre-polymer. Both components are viscous liquids.

b) The pre-polymer is poured over the master and takes the shape of its protruding channel structure with fidelity of 10s of nanometers.

c) For the curing process the setup has to be exposed to 70° C using an oven or a hotplate for 1 hour curing time.

d) Last but not least the PDMS channel can be peeled of the master. The peeled PDMS can be used as it is by just placing it over the desired surface and it will seal with the surface by itself and therefore it can be peeled off again and used multiple times. On the other hand it can also be permanently sealed over the sensor irreversibly. To do that the surface and the PDMS channel have to be exposed to Air-plasma for 1 min to generate silanol groups (Si-OH) on the PDMS surface by the oxidation of methyl groups.

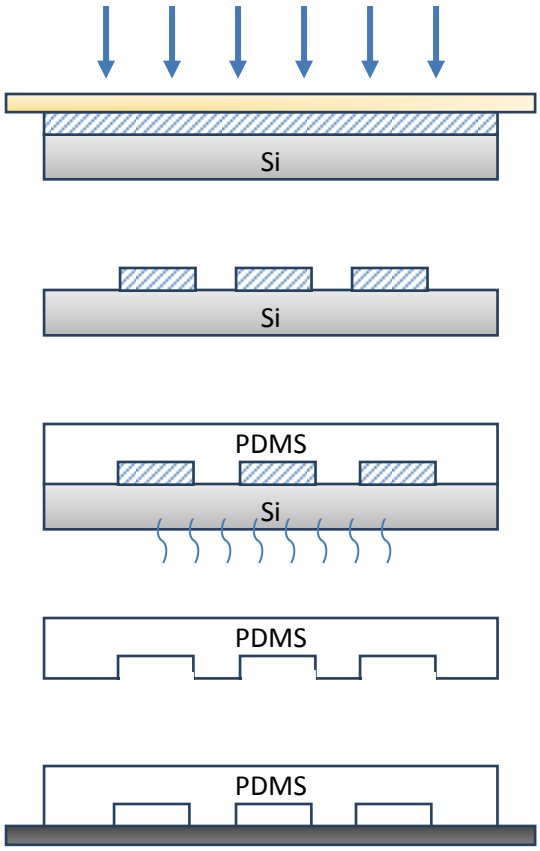

Figure 4.8: The standard steps of preparing a PDMS channel system. a) photo-lithography photoresist is exposed to UV light through the photomask. b) The extra PR is etched. c) PDMS is poured and cured at 70° C for 1 hour. d) PDMS is peeled gently. e) PDMS channel is placed over a flat surface and sealed [49].

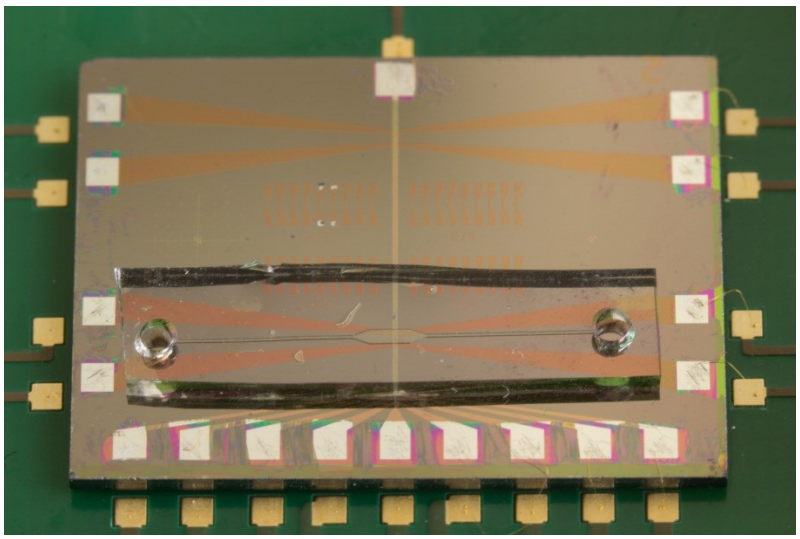

Figure 4.9: The sensor chip and the microfluidic channel placed on top with its inlet and outlet for sample introduction. In the middle there is the buffer where the two GMR sensors and the gold conductors exist.

4.2 Sample Preparation and Introduction

First experiments were carried out using samples consisting of deionized water (as a medium) and magnetic microparticles.

In order to prepare the right sample a water-particle mix with a ratio of 10:1 was used in order to create a medium where particles were not too dense or rare. This helped during sample observation under the microscope. To ensure a clean sample all mixing and preparation was carried out in a dust reduced or dust free chamber. All tools were kept in a laminar air flowbox after being desinfected and cleaned with some light alcohol to dissolve fats and othere contaminants that might disturb the sample during observation. Latex powderless gloves were used while carrying out the experiments.

The fluid sample was introduced inside the microfluidic channel from the inlet using a pipette. A syringe and a flexible pipe attached to it (see Figure 4.10.) were placed at the outlet in order to suck the fluid sample and ensure that the whole channel was filled with the sample. Specifically, a small amount of sample was dripped over the channel's inlet and the syringe was used to suck the sample from the other side (the outlet). The sample introduction should be made such that the sample is not flowing inside the channel but remains static, and to achieve that, any extra fluid should be sucked away from the inlet and the outlet (e.g. a tissue can remove any residual fluids in a gentle way). The reason of the unwanted flow is the difference in pressure between the channel's inlet and outlet resulted from extra sample fluid on either.

Figure 4.10: Shows the assembly of a syringe and a rubber tube which is used to bring the analyte sample inside the microfluidic channel. The rubber tube seals on the outlet of the channel and by applying a slight vacuum from the syringe the analyte sample will be sucked to its appropriate position inside the channel (i.e. the channel buffer).

4.3 Measurement Setup

In this section the electrical connections are explained & clarified in order to give a clear idea of how the overall experimental measurement is working. The GMR sensor was supplied with a certain frequency and the conductor laying over the sensor was supplied with another frequency; the resultant signal at the sum of those two frequencies was demodulated using a Lock-in Amplifier. The current carrying conductor was supplied with a current in the range between 20 to 50 mA depending on the conductor type and its ability to withstand a certain current for a long time of measurement. The GMR was supplied with a current of 0.8 mA. A Stanford Research Systems DSP lock-in amplifier measured the voltage around the GMR sensor (i.e measuring the current that the sensor consumes which is dependant to magnetic field change) and displays the RMS value of the voltage component at the frequency of $f_{sensor} + f_{conductor}$according to the modulation theorem [51]. In this setup the phase component was neglected since it has no contribution to the measured voltage output (setup shown in Figure 4.11.).

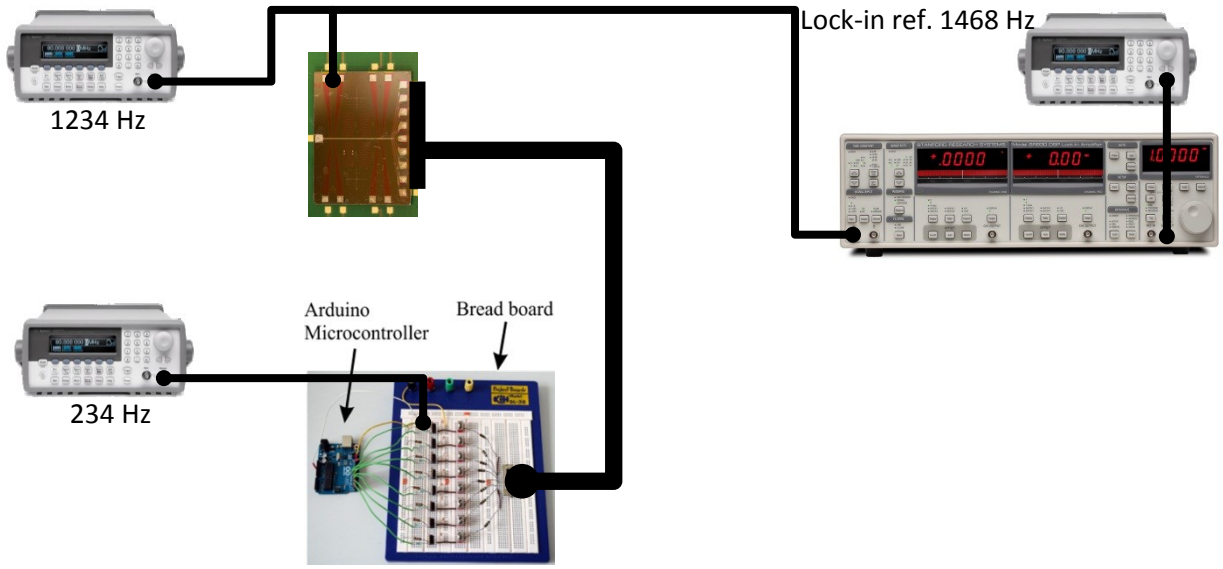

Figure 4.11: The basic experiment setup. At most left are two Agilent function generators that supply the GMR and the conductors, as previously discussed. The breadboard circuit with the Arduino chip is connected with a bus and used to power the conductors in two modes, an automatic mode used to control the 9 conductors and to switch them sequentially for nanomagnetic particles actuation and a manual mode in which individual conductors can be switched on and off for diagnoses and testing purposes. To the right the Stanford Lock-in amplifier displays the amplitude in the range of microvolts and a function generator is used to set the demodulation frequency (or reference frequency) at the sum of the system input frequencies.

4.3.1 Automation of the Measurement Setup

In order to create a portable measurement set-up a software solution combined with a computer's soundcard was developed and used to replace the bulky Lock-in amplifier.

The idea is to utilize the soundcard of any computer as a measurement input within the features that the soundcard is capable to handle; signals that are coming from the fabricated sensor are to be fed to the soundcard's line-in or microphone inputs with the standard range of ±1.0 Volts.

The characteristics of a Standard Soundcard Line-in are:

- A usual soundcard accepts a voltage input of ±1.0 Volts, however most soundcards can handle voltages over their limits up to ±2.5 Volts.

- An inherent component of a soundcard line-in is the ADC (Analog-Digital-Converter) which samples the data going into the soundcard inputs.

- Each sample can be quantized at 8, 16 or 24 bit depending on the soundcard quality.

- Sample rate capabilities can go up to 96000 Sample per second S/s.

- The typical input impedance is around 10.0 KΩ which is also considered as high impedance in comparison to the line-out which is 100 – 600 Ω. Figure 4.12 shows the typical soundcard channels and Figure 4.13 shows a block diagram of the system.

Figure 4.12: Typical soundcard channels left to right respectively (line-in, microphone and line-out).

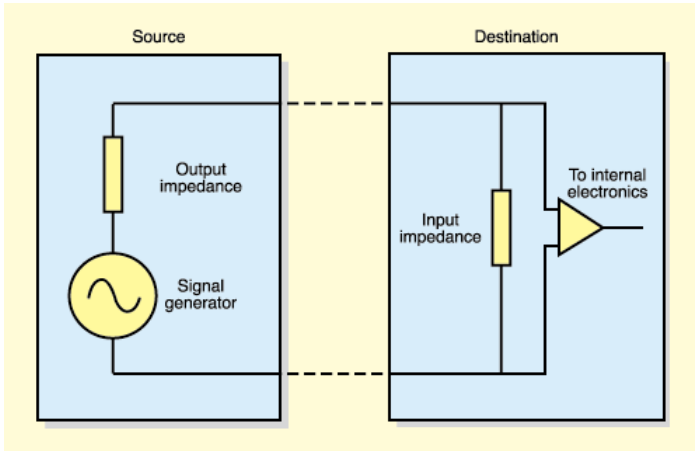

Figure 4.13: A block diagram showing the system impedances.

Figure 4.14 shows a circuit analysis of the typical impedances between the soundcard and an outside device.

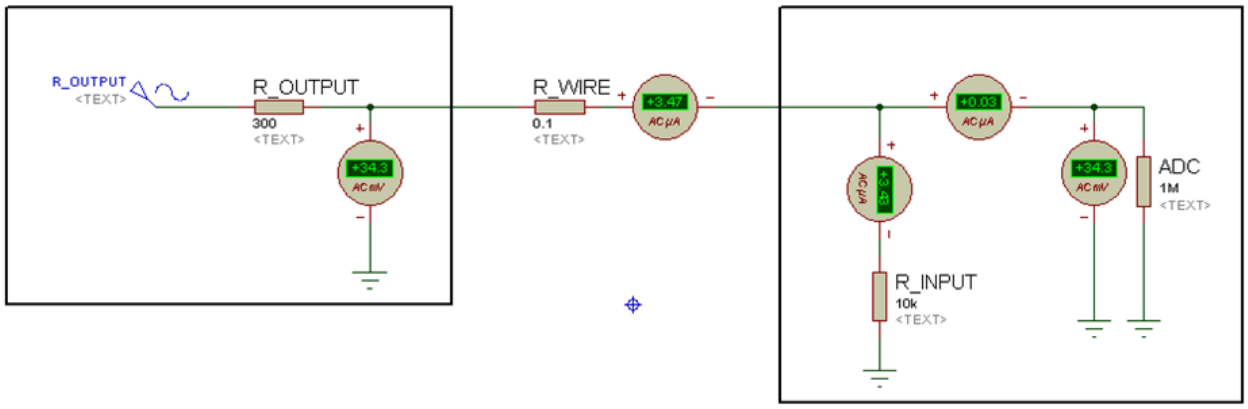

Figure 4.14: Simulation schematic of signal coupling to the soundcard considering the typical impedances.

In the developed measurement setup the following components are used:

- The soundcard itself, using the line-in channel which has a left and a right channel.

- a 3.5mm audio jack connector, a BNC connector and a coaxial cable to ensure good shielding against electromagnetic noise from neighboring devices.

- A simple voltage limiting circuit to protect the soundcard's line-in from potentially damaging overvoltage, which limits the voltage till ±0.6 Volts (see Figure 4.15).

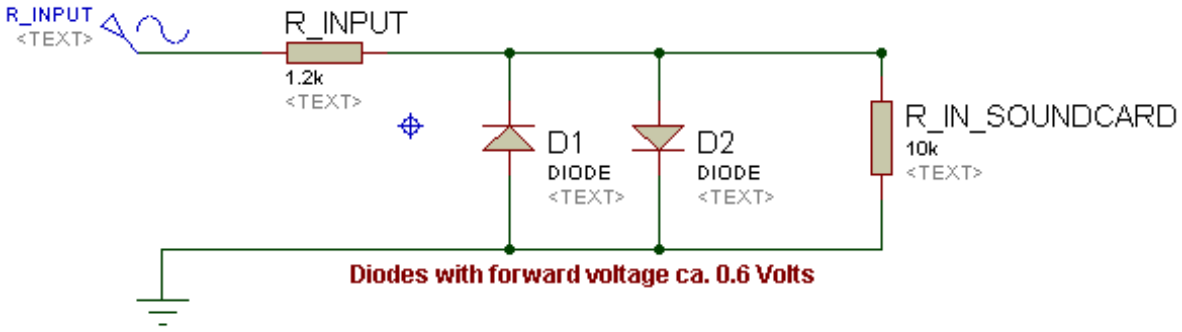

Figure 4.15: Voltage limiting circuit [52].

Soundcards come in different shapes and architectures depending on the usage and quality. The simplest and cheapest soundcard with a line-in input can do the measurement job in this project; however it is always important to know the different types and which ones are suited best for the required application. The very common sound devices are installed inside a PC as expansion cards on the motherboard PCI slots (Peripheral Component Interconnect), and they are quite durable and replaceable.

On the other hand portable computers (laptops) use an integrated sound chip placed on the motherboard which is a disadvantage in case sound chip damage. Therefore extra protection circuitry has to be used on the external feed line to ensure safety of the sound chip or as an alternative a USB stick sound device can also be used.

Figure 4.16 shows a passive circuit enclosed in a proper metal box; noise shielding is important in every passive and active element in the experiment setup.

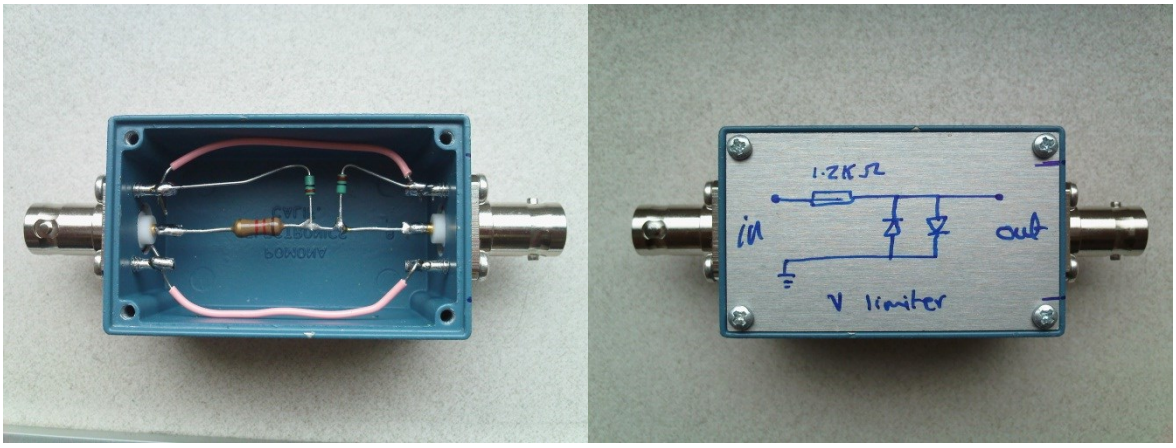

Figure 4.16: Shows a self-made voltage limiter circuit enclosed in an appropriate shielding.

- The measurement software consists of MATLAB code. For a real-time measurement data analysis and processing the MATLAB program accesses the soundcard through the soundcard driver in windows and performs acquisition to get what is available in the soundcard's buffer. With a few MATLAB code lines one can set the amount of data to be acquired and in which precision. The software tries to mimic the lock-in technique which the lock-in amplifier uses and therefore replacing the usage of a bulky expensive device as in the original measurement setup.

What the lock-in amplifier does is that it can extract the signal with a known carrier wave frequency which is buried in a noise that has larger amplitude by comparing the input signal to a strong reference signal which has the same frequency of the input signal. Then it performs low pass filtering with the ability to adjust the cutoff frequency of the filter. Figure 4.17 shows a simplified lock-in amplifier concept.

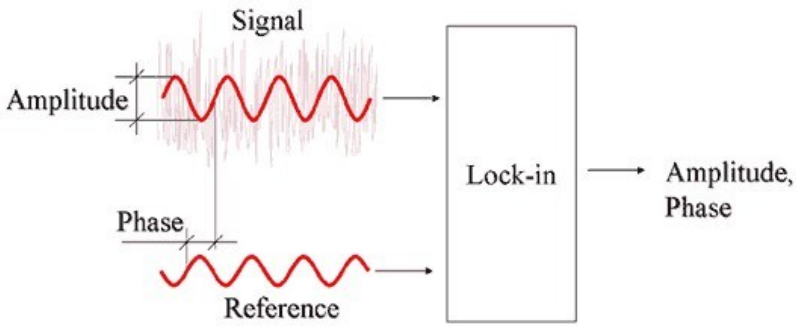

Figure 4.17: Shows a simplified schematic of Lock-in Amplifier

However, our software does not follow the conventional lock-in amplifier technique. Instead it uses FFT (Fast Fourier Transform) and software filtering; FFT converts the raw time-domain signal into a frequency-domain signal showing the intensity of each frequency in that signal. The resultant is a matrix with a set of complex numbers which comprise a real part which is the amplitude and an imaginary part which is the phase. The matrix indices are the frequencies detected in the range of the acquired sample rate (e.g. a sample rate of 8000 Sample/second will produce a matrix with 8000 complex elements). Figure 4.18 shows the output of the MATLAB program.

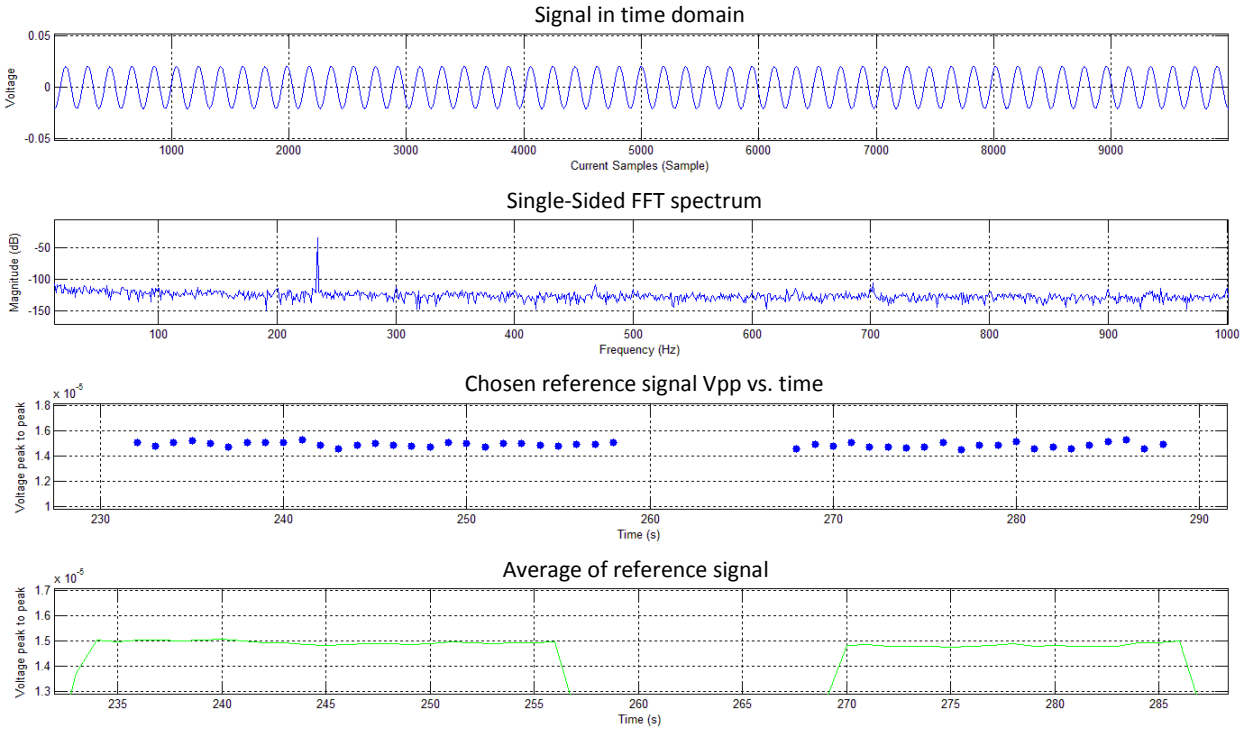

Figure 4.18: Output of the MATLAB program rescaled to show the important parts of the acquisition session. The top 1st graph plots the raw analog signal (time domain). The 2ndgraph plots the FFT (frequency domain) showing the dominating signal in the spectrum and noise spreading on the whole spectrum. The 3rdgraph plots the reference frequency from the FTT to view its change in time. The 4th graph plots the average of the 3rd graph to make changes overtime distinguishable. The two different plateaus show a very little difference, the first one shows a signal from the sensor and a particle over it while the second one shows only a the signal without the particle.

Three methods were developed for the measurement procedure. Due to software limitations and OS platform limitations, MATLAB is unable to read the sound data on all systems using one method. Therefore, different MATLAB data acquisitions methods were used; two involving the soundcard and the third using the "NI USB-6251 National Instruments DAQ". Below are the details of each method.

1) Data Acquisition using legacy devices (32-bit system only):

A legacy device is a device that does not belong to the Plug-and-play PnP type or devices which lack a peripheral controller. On a 32-bit MATLAB combined with a 32-bit or 64-bit operating system

(Windows), we can easily do it by using an analog input object *analoginput('winsound')*, one of the MATLAB's sound data acquisition functions [54].

2) Data Acquisition using Legacy devices (32 and 64 bit systems):

For this method we can use another non-standard object that MATLAB provides which is audio recorder (almost the same output but not from the Data Acquisition Toolbox) *audiorecorder(Fs,nBits,nChannels)* [55].

3) Data Acquisition using Session based devices (for National Instruments DAQ):

With NI one can get higher capabilities:
- Higher voltage limits ±10.0 Volts
- Higher sampling rate up to 1250000 S/s
- Precision of 16-bit for each sample
- Multiple analog and digital inputs and outputs and counters [56, 57].

Figure 4.19 shows the advantage of mobility and flexibility. In comparison with the specialized laboratory devices this NI module is still a disadvantage due to its limited data transfer which originate mainly from USB and computer software capabilities.

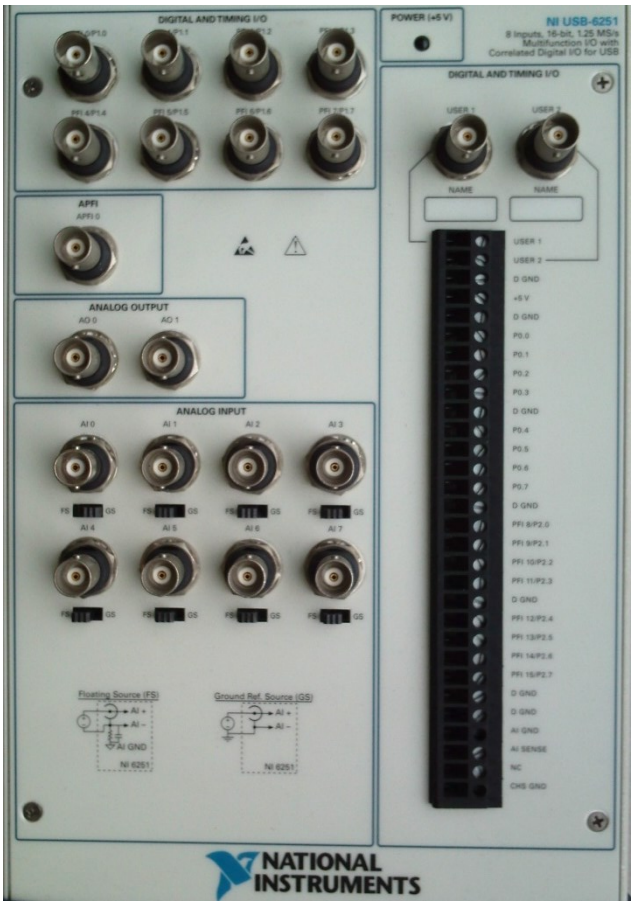

Figure 4.19: A USB multifunction I/O analogue and digital module from National Instruments which can be used almost as a miniaturized measurement and signal laboratory.

MATLAB which stands for (Matrix Laboratory) is a programming language developed by MathWorks; it allows matrix manipulations, functions and data plotting, algorithms and the creation of GUIs (Graphical User Interfaces). Beside that it can be interfaced with other programs written in other programming languages, including C, C++, Java and FORTRAN [58].

The implemented code in the thesis includes two files (or scripts); the first one is the main script and it deals with memory clearing, constants initialization, object creation and starting the program. The second script contains the code which will read the raw data from the soundcard buffer, process this data by performing computations and plotting. At the end, the script will save the results on the disk for later analysis. The program measures the data and displays analysis plotting in real time with a minimal rate of 1 second per measurement. Figure 4.20 shows a flowchart that represents the code algorithm. The code script can be found in the Appendix.

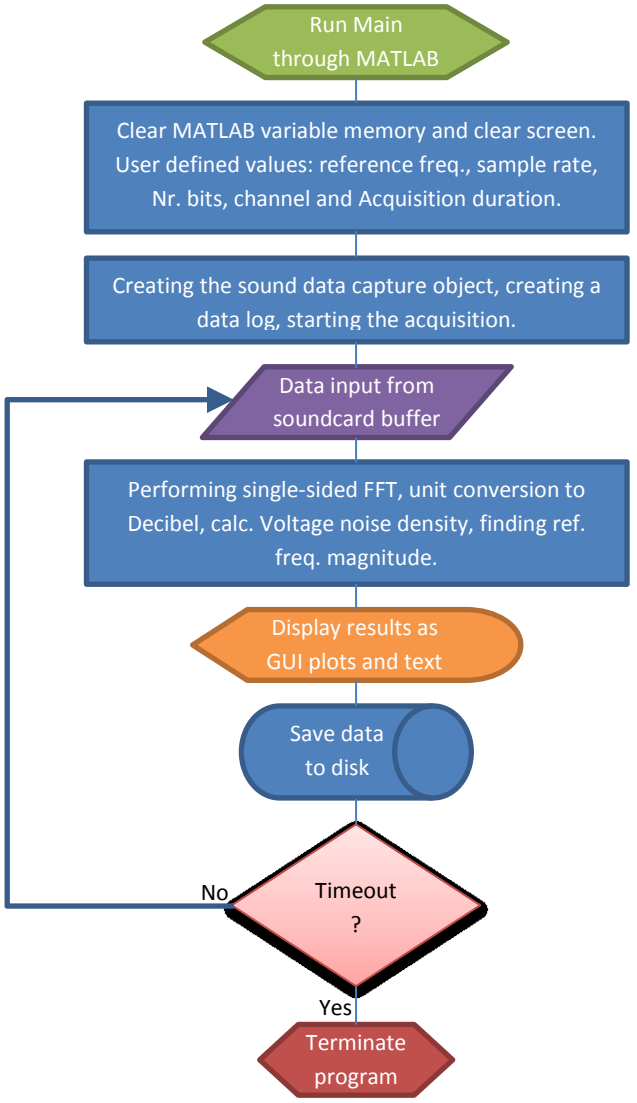

Figure 4.20: Algorithm which the MATLAB data acquisition program implements.

4.3.2 Power Control

As a requirement for a stable measurement system error sources should be minimized. In this project there are different sources of errors that can disrupt the measurement curve during operation; ambient temperature changes including room air currents can introduce such errors. Temperature changes affect the resistance of the used components (the conductors and GMR spin-valves), thus changing the consumed current of that element. A current control circuit has been proposed and implemented; it can source the conductors with their specific operating current and keep it constant even if temperature has changed. The implemented circuit uses the Howland Current Pump design principle.

The basic Howland pump was invented by Prof. Bradford Howland of MIT in 1962 and was first published in 1964. The pump can source currents in AC or DC and can force current into sensors or other elements; they can also be designed to drive varying loads with a wide range [59].

A typical aluminum conductor has a resistance of 69.7 Ω at room temperature and about 87.6 Ω at 100° C. The typical current consumption range is material dependant and can be chosen in the range of 20 to 50 mA. For a long experiment, the increased temperature due to current passing in the conductor material heat up the conductor including the sensor under it and the surroundings leading to measurement errors. Also passing current for a long time lead to conductor disintegration and wear. In this case the Howland Current Pump plays a significant role in limiting those effects (see Figure 4.21).

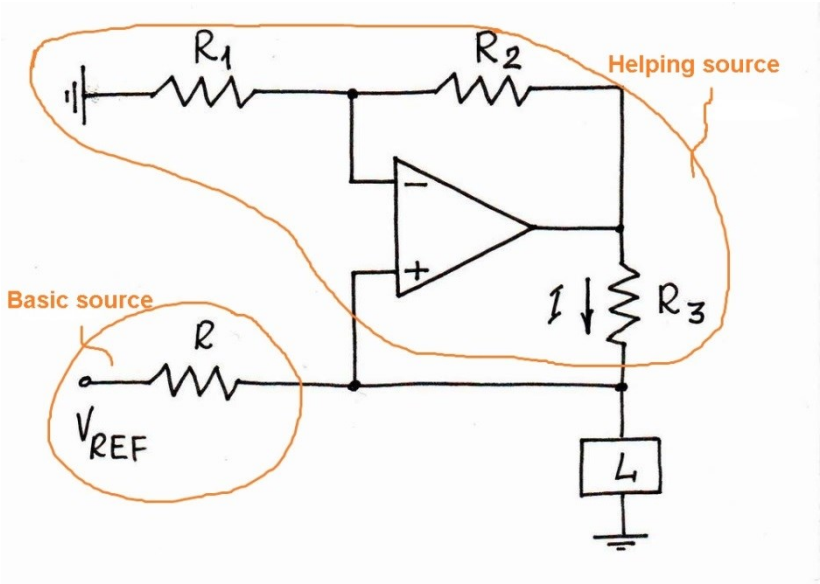

Figure 4.21: The Basic Howland Current Pump

In most applications $R_1 = R_2 = R_3 = R$, the resistors values and precision affect the circuit stability, so a good choice of resistors would be a matched tolerance and resistance. A reasonable tolerance value of the resistors is 1%, it is affordable and easy to find. However even more precise resistors can be used such as 0.1% and 0.01%. These are more expensive but give great stability [59].

In the following page the operation of Howland Current Pump, simulation and the implemented design will be explained.

Howland Current Pump is a solution for grounded loads (loads which are not floating); the idea is to source the load with a constant current by adding current. The circuit is composed of two main parts; a basic current source and a helping current source.

From Figure 4.21, V_{ref} and R form the basic current source, all other components R1, R2, R3 and the Opamp form the helping current source. The two sources meet at the node where the load L is connected. The Opamp will constantly sense any current changes over L and therefore source additional current to L. To calculate how much current is flowing through L the following derived formula is used [60]:

$$\boldsymbol{I_L} = \frac{\boldsymbol{V}}{\boldsymbol{R}} = \frac{V}{R} - \frac{V_L}{R} + \frac{V_L}{R}$$

Two parts are involved in the mentioned formula; they are simply derived from the two sources.

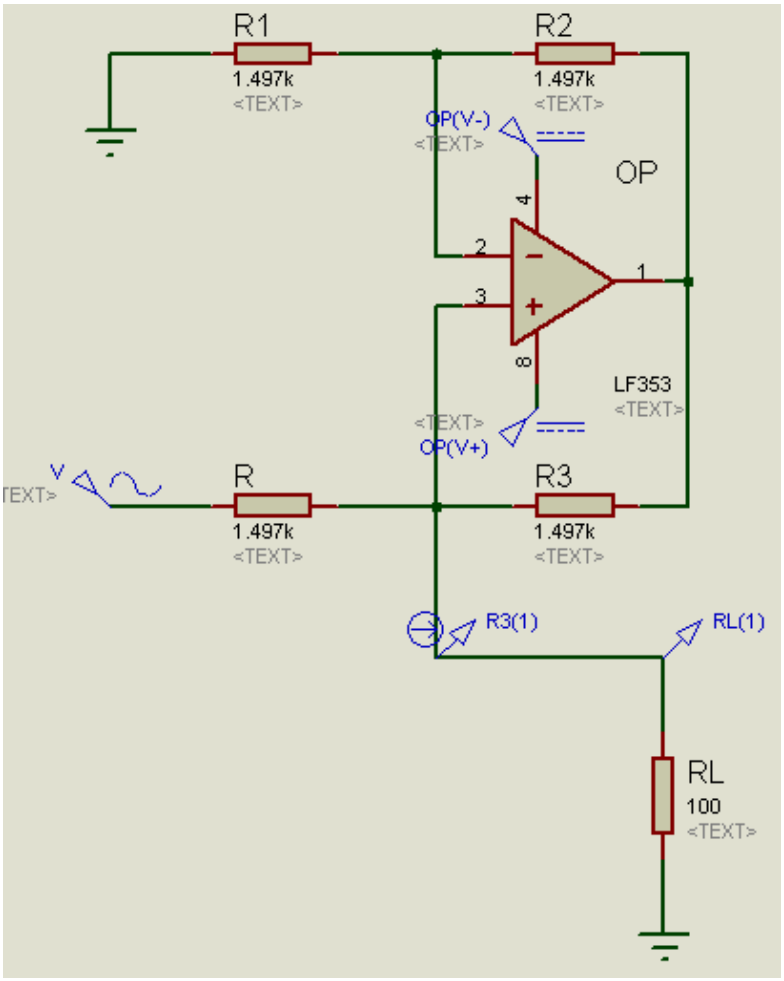

Figure 4.22: The implemented circuitry was simulated with Proteus Pro. software. Resistors values of 1.497 Ω and ±1% tolerance were chosen and the Opamp is of type LF353, it is powered by a TRACO DC-DC converter. LF353 is driven by ±15.0 Volts and it has an output voltage swing of ±12.0 Volts.

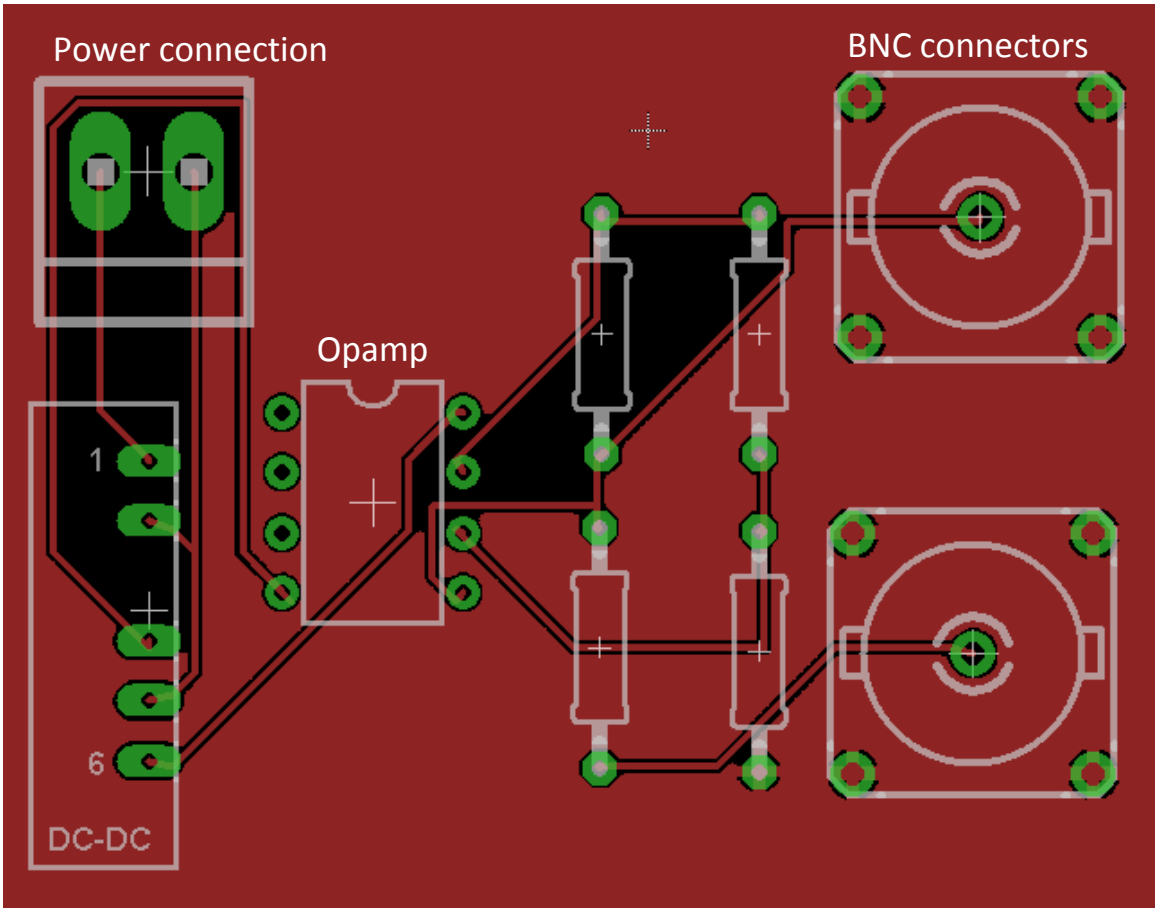

Figure 4.23: A circuit PCB board for the Howland Current Pump was designed using Eagle Light program. Circuit is about 5cm x 5cm and is enclosed inside a metal box to shield it against EMI.

4.4 Results and Conclusion

4.4.1 Single Particle Detection

Experiments were carried out with the set-up as described in Figure 4.11. to test if the GMR sensor is capable of detecting only one magnetic particle. Several challenges occur in this experiment; the first is to make the fluid stationary and to actuate it using the conductors, the second is to bring only one particle over the sensor area. To do that one has to experiment using trial and error and keep trying till one particle sits on the top of the sensor.

For a complete measurement and signal comparison, a measurement has to be taken with a bare sensor and a second measurement has to be taken with the particle over the sensor. After that the data saved from the MATLAB program can be imported by MS Excel, taking the averages of each peak and comparing them together to see the difference. Figure 4.24 shows amplitude difference of 4 µV was recorded.

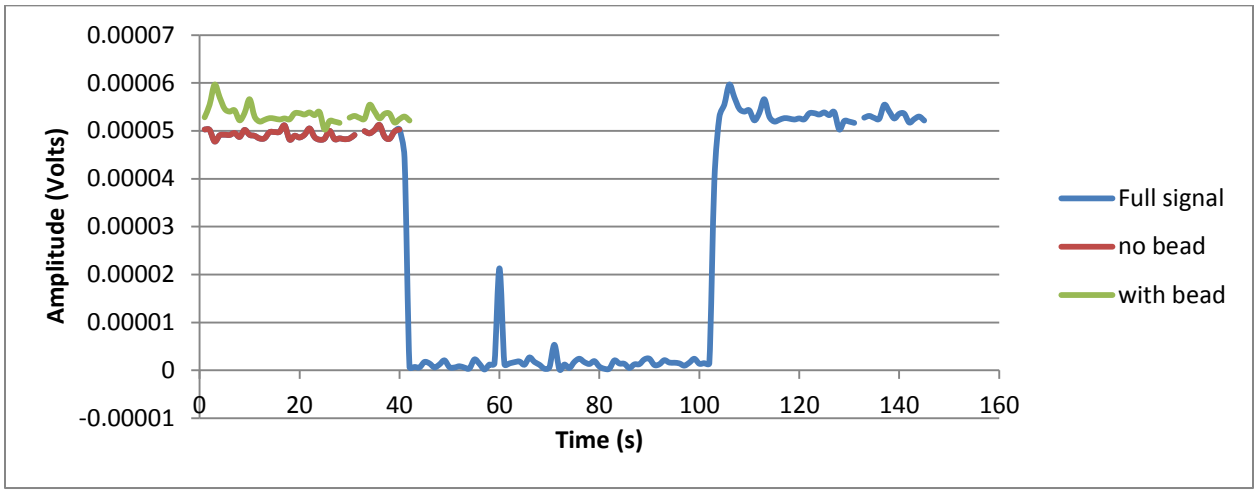

Without particle (x10^{-5})	With particle (x10^{-5})
5.0286907	5.2820455
5.0182211	5.5458320
4.7766866	5.9661236
4.9053343	5.7031956
4.9188251	5.4606668
4.9132083	5.4019243
4.9556837	5.4281109
4.8726089	5.2189490
5.0199660	5.3734749
4.9158771	5.6606533
4.8964189	5.2968793
4.8408274	5.1941528
4.8453158	5.2297509
4.9716465	5.2651435
4.9744839	5.2555117

4.9802732	5.2362978		
5.1139060	5.2591942		
4.8171044	5.2405069		
4.8971855	5.3657009		
4.8618164	5.3683540		
4.9198182	5.3406289		
5.0498799	5.3842711		
4.8684735	5.3274161		
4.8154149	5.3910679		
4.8369166	5.0283185		
5.0021451	5.2049590		
4.8268152	5.1927095		
4.8423745	5.1656903		
4.8254679	5.2745577		
4.8396520	5.3114084		
4.9140444	5.2701021		
4.9950070	5.2519081		
4.9474089	5.5447821		
5.0157758	5.4056190		
5.1225018	5.2582933		
4.8810868	5.3556543		
4.8328034	5.3589496		
4.9860018	5.1743494		
5.0275257	5.2443182		
	5.2977918		
	5.2153956		
Avg.	**Avg.**	difference	
4.9249537	5.3353819	4.1042825E-06	4μV
Percent of change	8.333646924%		

Figure 4.24: Shows values the MATLAB program measured, imported in MS Excel, plotted, tabulated and analyzed to show an amplitude difference of 4μV due to the increased magnetization volume of the GMR sensor of only one magnetic particle. Dynabeads® 280 (2.8μm) with streptavidin protein coating particles were used in this experiment.

4.4.2 Current Carrying Conductor as Temperature Sensor

The idea of using one of the particle actuation conductors as a temperature sensor for future setup improvement was tested. To do that the conductor has to be characterized by raising its temperature and measuring its resistance at different temperatures to create a temp-resistance curve, and eventually convert the resistance to temperature using the temperature coefficient equation. By using the formula $R(T) = R(T_0)(1 + \alpha\Delta T)$ we can convert the resistance to temperature; where R(T) is the resistance at a certain temperature (e.g. max temp.), $R(T_0)$ is the resistance at a reference temperature (e.g. min temp.), α is the temperature coefficient of the material (i.e. gold or aluminum … etc.) and ΔT is the difference between the reference and the requested temp.

The sensor was placed over a hotplate of 100° C and its resistance was precisely measured. Then the sensor was placed in the room temp. At 20.5° C and the resistance was again measured. To calculate the temperature of the sensor the resistances have to be plugged in the previous formula with α=0.04308 for aluminum conductor.

4.4.3 Proof of Concept

Experiments were conducted on the main sensor setup as a proof of concept of detecting MPs and LMPs when they pass over the GMR sensor while being magnetized using the current carrying conductors [34].

The used sensor has the following transfer curve as shown in Figure 4.25 showing a magnetoresistance ratio of 6.3%.

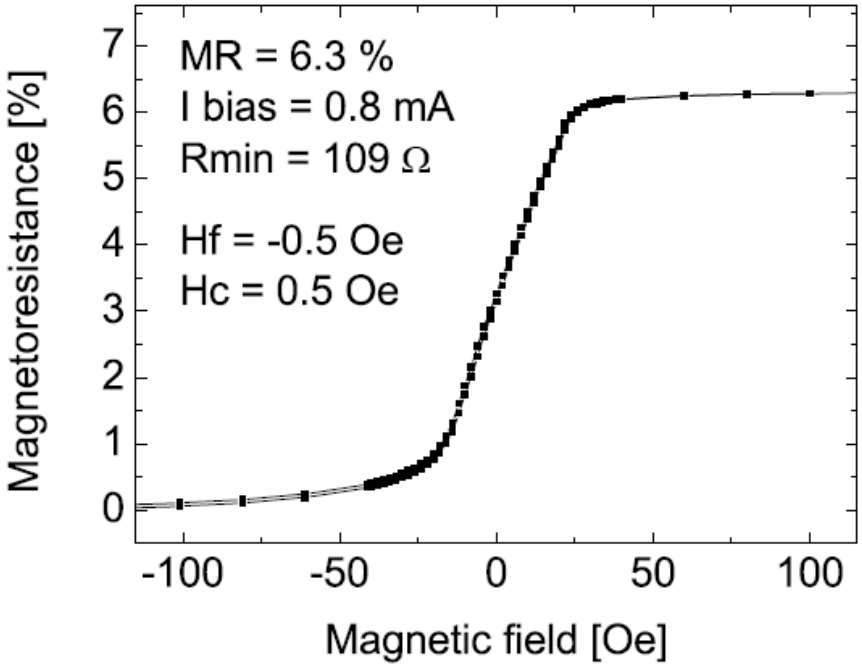

Figure 4.25: I_{bias} is the current that drives the GMR sensor, H_f is the field generated by the coupling ferromagnetic pinned layer, H_c is the coercivity field of the sensor [34].

The percentage of resistance change versus the increase was measured with a bare sensor (no MPs or LMPs), producing a field sensitivity of 0.12 %/Oe.

Magnetically tagged E.coli bacteria were used and introduced inside the detection microchannel and florescence microscopy was used to proof their passage over the sensor as shown in Figure 4.26. Afterwards the measurement system graphed the signal amplitude in Volts versus time using a lock-in amplifier and LabVIEW data acquisition software. The output of the lock-in amplifier was calculated theoretically in previous steps giving a signal of 339 μV. Figure 4.27 shows the measurement graph and a peak signal of 358 μV which is approximately similar to the theoretical outcome [34].

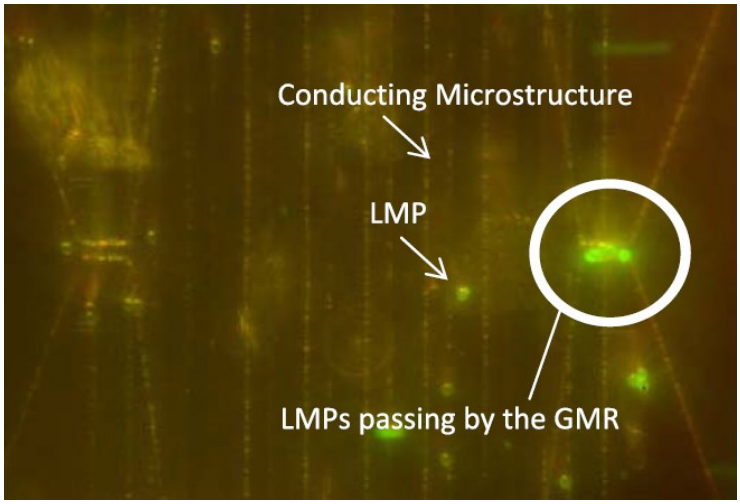

Figure 4.26: Fluorescently dyed E.coli LMPs are shown accumulating over the GMR sensor area, after they are detected by the first sensor they will continue moving using the DC current conducting structures until the opposite sensor detects them [34].

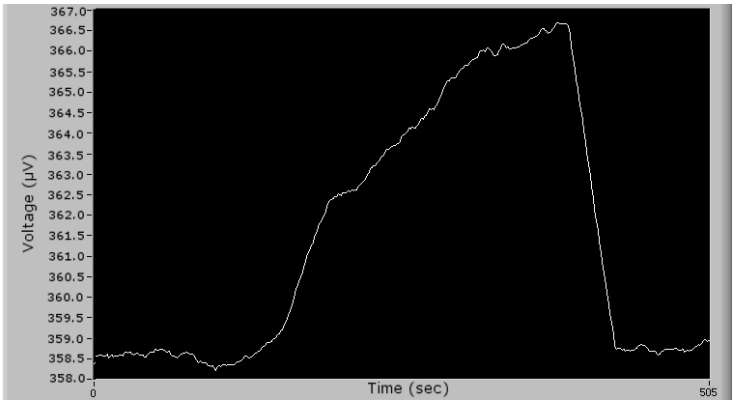

Figure 4.27: A signal graph vs. time showing how the LMPs are accumulated together increasing the magnetic volume of the sensor [34].

5. Conclusion and Outlook

In this thesis a microfluidic biosensing device using a GMR sensor system and magnetic particles (MPs) for pathogen detection was described. The device is composed of two pairs of GMR sensors, current carrying conductors and two microfluidic channels. The current carrying conductors are used to accelerate the loaded magnetic particles (LMPs comprised of functionalized MPs with pathogens attached to their surface) in the main detection channel and also to accelerate the MPs in the reference microfluidic channel. The current carrying conductors generate a gradient magnetic field around each of them. By switching them on and off sequentially a continuous MPs and LMPs motion occurs. The reference microfluidic channel constantly measures the velocity of the bare MPs, thus giving the ability to reduce errors. Analytical calculations were presented to clarify the MPs and LMPs motion principles.

A new method was developed and introduced as a new measurement system to replace a bulk and expensive solution, which is, replacing the lock-in amplifier with computer software made on MATLAB and using the computer's soundcard as a signal input. Additional control units were implemented; a current control for the system to deal with thermal fluctuations effect on the devices resistances and an indirect temperature sensor by using one of the current carrying conductors. Finally, experiments were conducted to prove the ability of the sensor to detect one single MP and magnetically labeled *E. coli.* With the mentioned points the aim of this thesis was fulfilled successfully.

The next step of this research project is to implement more automation techniques in order to fully automate the operation and measurement of the biosensing system.

Appendix

PDMS base + curing agent:

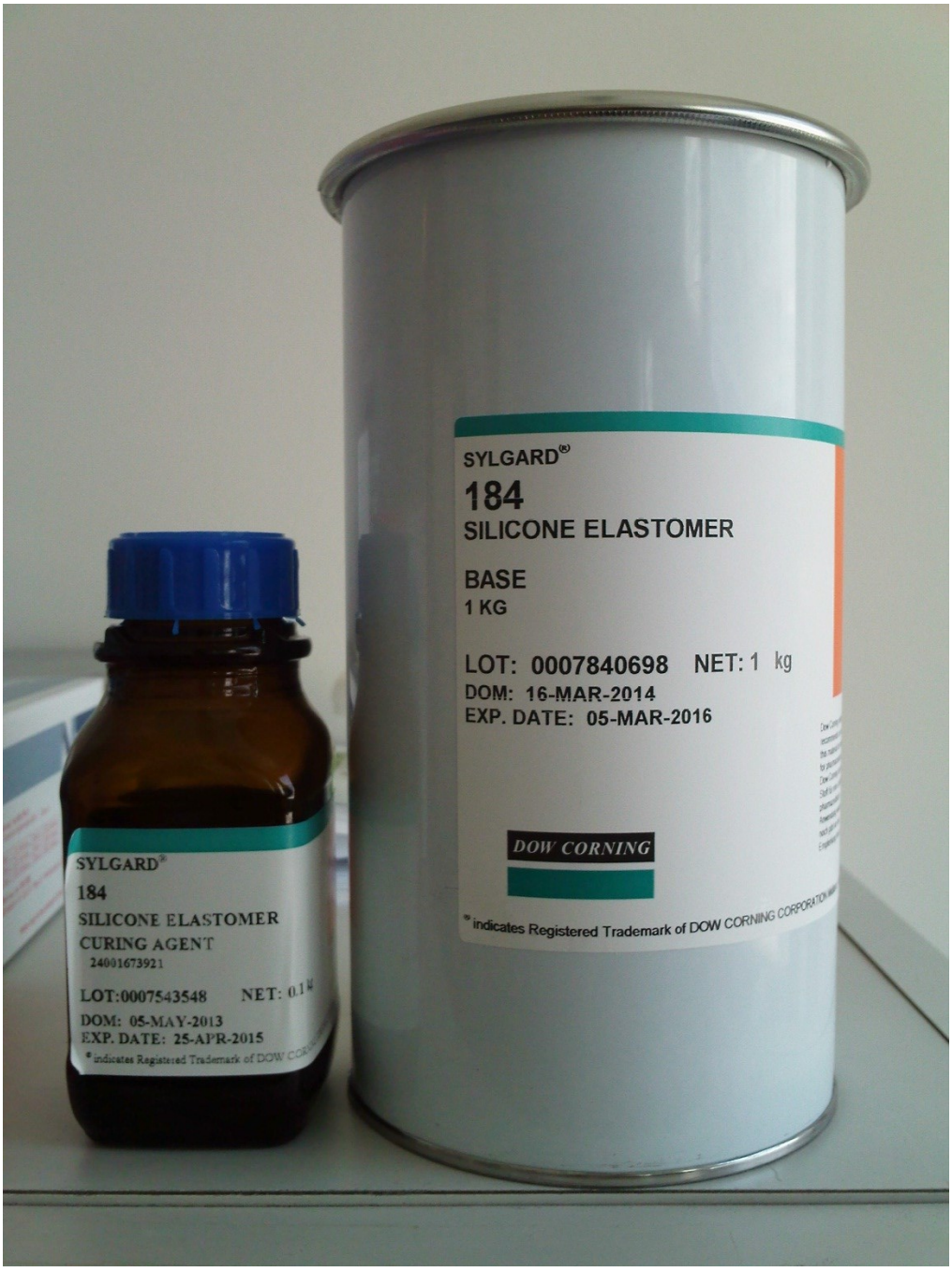

Figure A.1: Shows the PDMS base + curing agent

Magnetic Nanoparticles:

Ligand	Target	Dynabeads® Epoxy	Dynabeads® Tosylactivated	Dynabeads® Carboxylic Acid	Dynabeads® Amine
Antibody	Low MW antigen[1] or peptide	●●	●●●	●●	●●
	Protein or antibody[2]	●●●	●●●	●●	●
	Protein complex	●●●	●●	●	●
	Organelle	●●[3]	●●		
	Phage[1]	●●	●●●	●●	●●
	Virus	●●	●●●	●●	●●
	Bacteria		●●●		
	Cells[4]	●●●	●●●		
Antibody fragment	Phage[1] or antibody	●●	●●	●●●	●●●
Protein	Phage[1] or carbohydrate	●●●	●●	●●	●●
	Nucleic acid	●	●	●●●	●
Peptide	Phage[1] or antibody	●●	●●	●●●	●●●
Carbohydrate	Antibody	●		●	●●●
Low MW antigen	Antibody	●●	●●	●●	●●
Nucleic acid, oligonucleotide, aptamer, PNA	Nucleic acid binding proteins[1]		●	●●	●[5]
	DNA,[1] RNA,[1] or PCR amplicons[1]			●●●	●[5]
Enzyme	Substrate or target for enzyme degradation	●●●	●●	●	●
Organic chemistry derivatization, including introduction of new functional groups		●●	●●	●●	●●●

••• Best product choice for listed ligand and target
•• Alternative choice for listed ligand and target
• Can be used for listed ligand and target
[1] Dynabeads® precoupled with streptavidin may be the best product choice.
[2] Dynabeads® Antibody Coupling Kit contains Dynabeads® M-270 Epoxy and buffers required for covalent coupling.
[3] Dynabeads® M-450 Epoxy
[4] Dynabeads® M-450 are recommended for isolation, activation, and expansion of cells.
[5] Dynabeads® Amine are modified with an appropriate bifunctional crosslinker prior to immobilization of oligonucleotides.

Figure A.2: Shows the used Magnetic particles specification sheet.

CAD design of the sensor wafer masks layered:

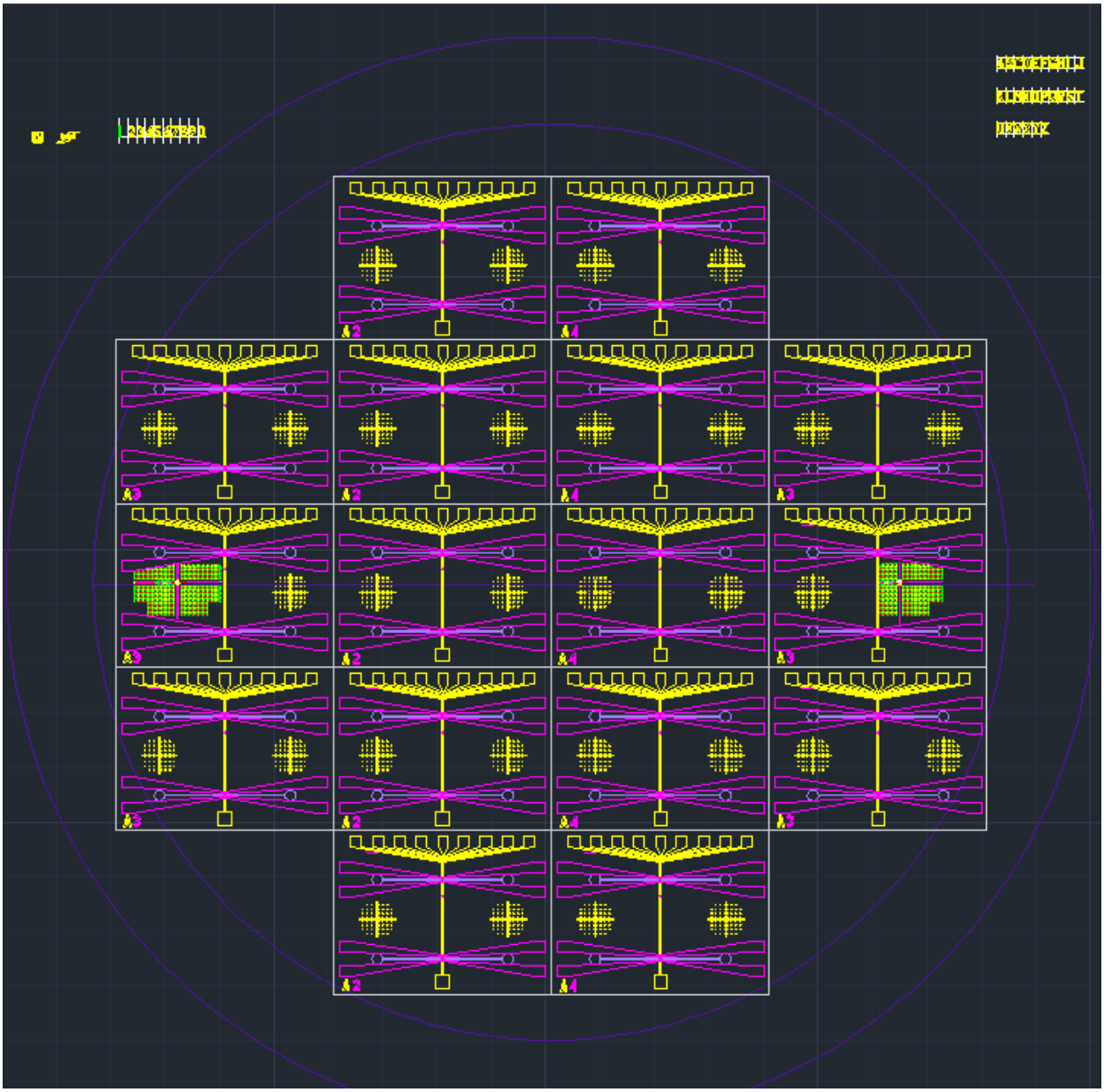

Figure A.3: Shows an AutoCAD® design for the GMR sensors

The MATLAB program code which is used to acquire the data and produce a measurement curve

First Program

Main module

```
%Programmed by: BSc. Murad Jamalieh
%-----------------------------------------------------------------------

% Main Program
% works on all systems (32,64 bit) using the audiorecorder
functionality
% Calibration of soundcard line-in volume is nessesary to match a
reference
% measurement instrument (e.g a Lock-in amplifier)

% emptying any old buffers and graphics
clc
clf
clear all

reference_freq = 1468 % ref. freq(Hz) that we want to measure its
amplitude
fs = 44100; % Sampling frequency in Hz (depending on soundcard
capability)
nbits = 24; % number of bits
acq_ch = 2; % acquisition channel (microphone, line-in)
duration = 5*60; % total duration of acquisition
timer_period = 1; % how often the timer function is triggered
% (1s is recommended)

% creating object for recording
lineinput = audiorecorder(fs, nbits, acq_ch);
% the TimerFcn refer to the recording function which perform the
aquisition
% and data analysis when recordblocking() function is called.
set(lineinput, 'TimerFcn', {@recording, reference_freq, duration}, ...
    'TimerPeriod', timer_period);

% write to file the beginning of each acquisition
fid = fopen('measurement_log.txt', 'a');
%write to log file
fprintf(fid, ['V_N_D', 32,32,32,32,32,32,32,32,32,32, 'Ref_amp',
32,32,32,32,32,32,32,32, 'amp_highestmag' , 32,32,32,32,
datestr(clock), '\n']);
%close the log file object
fclose(fid);

% starting to record
recordblocking(lineinput, duration);
```

Function Module

```
%Programmed by: BSc. Murad Jamalieh
%-----------------------------------------------------------------------

function recording(obj, event, reference_freq, duration)
%open or create a text file for logging data
fid = fopen('measurement_log.txt', 'a');
% Variables which their values are kept even if the function exits
% (static variables)
persistent r_m;
persistent r_m_avg;
persistent counter;

%time counter initialization
if isempty(counter)
    counter = 1;
else
    counter = counter + 1;
end

sample_rate = obj.SampleRate; % the current sample rate the object is
using
data = getaudiodata(obj); % getaudiodata accumulates the recorded data
% for the total duration

%taking all rows from the second column->left channel of the line-in
raw_data = data(:, 2);

% if statement to fix the first sample(undersampling) problem
if length(raw_data) >= sample_rate
    % get the last e.g. 8000 samples from the buffer
    % because audiorecorder accumulates data in one buffer!!
    raw_data = raw_data(end-sample_rate+1:end);
else
    % get the last samples in case they are smaller than the sample
rate
    % from the buffer, because audiorecorder accumulates data in one
buffer
    raw_data = raw_data(end-length(raw_data)+1:end);
end

display(['Iteration:' num2str(counter) 13 'Data Length Per Sample:'
...
    num2str(length(raw_data))])

%raw signal
figure(1)
subplot(4,1,1);
plot(raw_data)
title('Signal in Time domain')
ylim([-0.5 0.5]);
```

```
xlabel('Current Samples (Sample)')
ylabel('Voltage')
grid on;

%Fast Fourier Transform to get the frequency information
%FFT is sensitive to NaNs if there is one NaN then all the FFT result
is
%NaNs
% 1/N, N:data length, Averaging factor
fft1 = fft(raw_data)/(length(raw_data));
xfft = 2*abs(fft1); % FFT originally mirrors the spectrum and divides
the
% amplitudes over the symmetrical part and to get the original value
we
% multiply by 2

%convert the FFT result into a Decibel magnitude FFT
mag = 20*log10(xfft);
mag = mag(1:int32(end/2)); % getting the single sided FFT

f = (0:length(mag)-1);
subplot(4,1,2)
plot(f,mag)
%axis([1460 1480 -Inf 0]);
axis([0 sample_rate/2 -Inf 0]);
title('Single-Sided FFT Spectrum')
xlabel('Frequency (Hz)')
ylabel('Magnitude (dB)')
grid on;

%Voltage noise density
vnd = rms(raw_data(1:int32(end/2)))/sqrt(sample_rate);

display(['Voltage_Noise_Density:', 32, ...
    num2str(vnd), ...
    32,'Vrms/sqrt(Hz)'])

%reference frequency magnitude
r_m = [r_m db2mag(mag(reference_freq + 1))];
r_m_avg = smooth(r_m);
display(['Ref_Magnitude:', 32, num2str(r_m(end)), 32,'Vpp'])

[db, freq] = max(mag); %getting the freq(index) of the highest
magnitude.
display(['Magnitude_Highest_Power_Freq:', 32, ...
    num2str(db2mag(db)), 32, 'Vpp'])
display(['freq:', 32, num2str(freq-1), 32, 'Hz'])
% frequency index is subtracted by 1 because FFT values correspond to
data
% starts from 0 and MATLAB indexing starts from 1

%write to log file
```

```
fprintf(fid, '%1.12f %1.12f %1.12f\n', [vnd r_m(end) db2mag(db)]);
%close the log file object
fclose(fid);

subplot(4,1,3)
plot(r_m, '.', 'MarkerSize', 20)
xlim([0 duration-1]);
title('Chosen signal(Reference) Vpp vs. time')
xlabel('Time (s)')
ylabel('Voltage peak to peak')
grid on;

subplot(4,1,4)
plot(r_m_avg, '-g')
xlim([0 duration-1]);
%ylim([0 1e-03]);
title('Average of reference')
xlabel('Time (s)')
ylabel('Voltage peak to peak')
grid on;

display('-----------------------------------------------------------------
---')
end
```

List of Figures

Figure A.3: Shows an AutoCAD® design for the GMR sensors.

List of Tables

Bibliography

[1] I. Giouroudi, F. Keplinger. "Microfluidic biosensing Systems using Magnetic Nanoparticles"; International Journal of Molecular Sciences, 14 (9), 18535-18556, doi: 10.3

[2] Varadan, V.K.; Chen, L.; Xie, J.Nanomedicine: Design and Applications of Magnetic Nanomaterials, Nanosensors and Nanosystems; John Wiley & Sons, Ltd.: West Sussex, UK, 2008.

[3] Guimaraes, A.P. Principles of Nanomagnetism; Springer: Berlin, Heidelberg, Germany, 2009.

[4] Bean, C.P.; Livingston, J.D. Superparamagnetism. J. Appl. Phys. 1959, 30, 120–129.

[5] Indira, T.K.; Lakshmi, P.K. Magnetic nanoparticles—A review. Int. J. Pharm. Sci. Nanotechnol. 2010, 3, 1035–1042.

[6] Tran, N.; Webster, T.J. Magnetic nanoparticles: Biomedical applications and challenges. J. Mater. Chem. 2010, 20, 8760–8767.

[7] Hristoforou, E. Magnetic effects in physical sensor design. J. Opt. Adv. Mat. 2002, 4, 245–260.

[8] Melancon, M.; Lu, W.; Li, C. Gold-based magneto/optical nanostructures: Challenges for in vivo applications in cancer diagnostics and therapy. Mater. Res. Bull. 2009, 34, 415–421.

[9] Bumb, A.; Brechbiel, M.W.; Choyke, P.L.; Fugger, L.; Eggeman, A.; Prabhakaran, D.; Hutchinson, J.; Dobson, P.J. Synthesis and characterization of ultra-small superparamagnetic iron oxide nanoparticles thinly coated with silica. Nanotechnology 2008, 19, 335601.

[10] Li, G.X.; Sun, S.H.; Wilson, R.J.; White, R.L.; Pourmand, N.; Wang, S. Spin valve sensors for ultrasensitive detection of superparamagnetic nanoparticles for biological applications. Sens. Actuators A 2006, 126, 98–106.

[11] Samal, D.; Kumar, P.S.A. Giant magnetoresistance. Resonance 2008, 13, 343–354.

[12] Weber, E.; Vellekoop, M. Optofluidic micro-sensors for the determination of liquid concentrations. Lab Chip 2012, 1219, 3754–3759.

[13] Nickel, J. Magnetoresitance overview. HP Labs 1995, Available online: http://www.hpl.hp.com/techreports/95/HPL-95-60.pdf (accessed on 26 July 2013).

[14] Ripka, P. Magnetic Sensors and Magnetometers; Artech House Publishers: Boston, UK, 2001.

[15] Freitas, P.P.; Ferreira, R.; Cardoso, S.; Cardoso, F. Magnetoresistive sensors. J. Phys. Condens. Matter 2007, 19, 165221.

[16] Ennen, I.; Albon, C.; Weddemann, A.; Auge, A.; Hedwig, P.; Wittbracht, F.; Regtmeier, A.-K.; Akemeier, D. From magnetic nanoparticles to magnetoresistive biosensors. Acta Phys. Pol. A 2012, 121, 420–425.

[17] Gaster, R.S.; Xu, L.; Han, S.J.; Wilson, R.J.; Hall, D.A.; Osterfeld, S.J.; Yu, H.; Wang, S.X. Quantification of protein interactions and solution transport using high-density GMR sensor arrays. Nat. Nanotechnol 2011, 6, 314–320.

[18] Xu, L.; Yu, H.; Akhras, M.S.; Han, S.-J.; Osterfeld, S.; White, R.L.; Pourmand, N.; Wang, S.X. Giant magnetoresistive biochip for DNA detection and HPV genotyping. Biosens. Bioelectron 2008, 24, 99–103.

[19] Giouroudi, I.; van den Driesche, S.; Kosel, J.; Grössinger, R.; Vellekoop, M. On-chip bio-analyte detection utilizing the velocity of magnetic microparticles in a fluid. J. Appl. Phys 2011, 109, 07. B304.

[20] Gooneratne, C.; Liang, C.; Giouroudi, I.; Kosel, J. An integrated micro-chip for rapid detection of magnetic particles. J. Appl. Phys 2012, 111, 07. B327.

[21] Li, F.; Giouroudi, I.; Kosel, J. A biodetection method using magnetic particles and micro traps. J. Appl. Phys 2012, 111, 07. B328.

[22] Manteca, A.; Mujika, M.; Arana, S. GMR sensors: Magnetoresistive behaviour optimization for biological detection by means of superparamagnetic nanoparticles. Biosens. Bioelectron 2011, 26, 3705–3709.

[23] Graham, D.L.; Ferreira, H.A.; Freitas, P.P. Magnetoresistive-based biosensors and biochips. Trends Biotechnol. 2004, 22, doi:10.1016/j.tibtech.2004.06.006.

[24] Reig, C.; Cubells-Beltrán, M.D.; Ramírez Muñoz, D. Magnetic field sensors based on giant magnetoresistance (GMR) technology: Applications in electrical current sensing. Sensors 2009, 9, 7919–7942.

[25] Giant Magnetoresistance Materials and Their Potential as Read Head Sensors Robert L. White Department of Materials Science and Engineering Stanford University, Stanford, CA 94305, IEEE Transactions On Magnetics, vol. 30. No. 2, March 1994.

[26] Magnetophoresis: http://www.springerreference.com/docs/html/chapterdbid/67081.html (accessed on 10 September 2014).

[27] Microfluidic cell culture Matthias Mehling and Savas, Tay.

[28] Tabeling, P. (2005). Introduction to Microfluidics. Oxford University Press.

[29] Physics and Applications of Microfluidics in Biology, Beebe. , Laminar Flow.

[30] N.-T. Nguyen and S. T. Wereley, Fundamentals and Applications of Microfluidics, Artech House, Inc., 2002.

[31] A. Dangl, G. Kokkinis, F. Keplinger, I. Giouroudi, "In vitro biosensing based on magnetically induced motion of magnetic nanoparticles"; Proc. Nanotech Conference & Expo 2013, Vol. 3,ISBN: 978-1-4822-0586-2; S. 135 - 138., Washington, USA, May 2013.

[32] G. Kokkinis, A. Dangl, F. Keplinger, I.Giouroudi, "Microfluidic biosensing method using the motion of magnetic microparticles" Key Engineering Materials Vol. 605, pp 348-351, DOI:10.4028/www.scientific.net/KEM.605.348, 2014.

[33] G. Kokkinis, F. Keplinger, I.Giouroudi. "On-Chip Microfluidic Biosensor using Superparamagnetic Microparticles", Biomicrofluidics, 7, 5; S. 054117-1 - 054117-14, 2013.

[34] G. Kokkinis, S. Cardoso, F. A. Cardoso, I.Giouroudi, "Microfluidics for the Rapid Detection of Pathogens using Giant Magnetoresistance Sensors" accepted for publication IEEE Transactions on Magnetics, 2014.

[35] Documented from the Institute of sensor and actuator systems, Technical University of Vienna (ISAS TUwien).

[36] M. Julliere (1975). "Tunneling between ferromagnetic films". Phys. Lett.54A: 225–226. Bibcode:1975PhLA...54..225J. doi:10.1016/0375-9601(75)90174-7.

[37] S. Ikeda, J. Hayakawa, Y. Ashizawa, Y.M. Lee, K. Miura, H. Hasegawa, M. Tsunoda, F. Matsukura and H. Ohno (2008). "Tunnel magnetoresistance of 604% at 300 K by suppression of Ta diffusion in CoFeB/MgO/CoFeB pseudo-spin-valves annealed at high temperature". Appl. Phys. Lett.93 (8): 082508. Bibcode:2008ApPhL..93h2508I. doi:10.1063/1.2976435.

[38] Introduction to TMR Magnetic Sensors http://www.dowaytech.com/en/e/action/ShowInfo.php?classid=10&id=92 (accessed on 11 September 2014)

[39] Nemat-Nasser, Sia; Isaacs, Jon B.; Liu, Mingqi (1998). "Microstructure of high-strain, high-strain-rate deformed tantalum". Acta Materialia 46 (4): 1307. doi:10.1016/S1359-6454(97)00746-5.

[40] Walters, William; Cooch, William; Burkins, Matthew (2001). "The penetration resistance of a titanium alloy against jets from tantalum shaped charge liners". *International Journal of Impact Engineering* **26**: 823. doi:10.1016/S0734-743X(01)00135-X.

[41] Russell, Alan M.; Lee, Kok Loong (2005). *Structure-property relations in nonferrous metals*. Hoboken, NJ: Wiley-Interscience. p. 218. ISBN 978-0-471-64952-6.

[42] Gerald L. Burke (1940). "The Corrosion of Metals in Tissues; and An Introduction to Tantalum". *Canadian Medical Association Journal* **43**.

[43] Elmen, G.W.; H. D. Arnold (July 1923). "Permalloy, A New Magnetic Material of Very High Permeability". *Bell System Tech. J.* (USA: American Tel. & Tel.) **2** (3): 101–111. Retrieved December 6, 2012.

[44] Jiles, David (1998). *Introduction to Magnetism and Magnetic Materials*. CRC Press. p. 354. ISBN 0-412-79860-3.

[45] Permalloy http://en.wikipedia.org/wiki/Permalloy

[46] High Temperature Pinning Properties of IrMn vs. FeMn in Spin Valves, Jul/*Aug 1999 Journal of*

Vacuum Science and Technology by the American Vacuum Society.

[47] The Spin Valve http://www.stoner.leeds.ac.uk/Research/TutSpinValve

[48] Magnetic Thermal Annealing: An Effective Process to Enhance the Performance of Magnetic Devices and Materials, Micromagnetics- sensible solutions. http://www.directvacuum.com/PDF/anneal.pdf (accessed on 11 September 2014).

[49] Poly(dimethylsiloxane) as a Material for Fabricating Microfluidic Devices J. COOPER MCDONALD AND GEORGE M. WHITESIDES Department of Chemistry and Chemical Biology, Harvard University.

[50] Hans-Heinrich Moretto, Manfred Schulze, Gebhard Wagner, "Silicones" Ullmann's Encyclopedia of Industrial Chemistry, 2005, Wiley-VCH, Weinheim.

[51] Bracewell, R. "Modulation Theorem." The Fourier Transform and Its Applications, 3rd ed. New York: McGraw-Hill, p. 108, 1999.

[52] Sound Card Input Range and Limiter Circuits http://www.daqarta.com/dw_0all.htm

[53] Matlab, MathWorks documentation portal, Choose the Right Interface http://www.mathworks.de/de/help/daq/choose-the-right-interface.html (accessed on 11 September 2014).

[54] Data acquisition toolbox MathWorks portal http://www.mathworks.de/products/daq/features.html (accessed 11 September 2014).

[55] About audio recorder implementation http://www.mathworks.de/de/help/matlab/ref/audiorecorder.html (accessed 11 September 2014).

[56] Session based interface MathWorks portal http://www.mathworks.de/de/help/daq/session-based-interface.html (accessed 11 September 2014).

[57] Acquiring data using National Instruments devices http://www.mathworks.de/de/help/daq/examples/acquire-data-using-ni-devices.html (accessed 11 September 2014).

[58] MATLAB Wikipedia http://en.wikipedia.org/wiki/MATLAB (accessed 11 September 2014).

[59] AN-1515 a comprehensive study of the Howland current pump, Texas Instruments, SNOA474A January 2008–Revised April 2013.

[60] Howland Current Source for Grounded Load http://www.circuit-fantasia.com/circuit_stories/understanding_circuits/current_source/howland_current_source/howland_current_source.htm (accessed 11 September 2014).